Multidimensional visualization of preferential flow pathways using neutron and x-ray radiation

Von der Fakultät für Umwelt und Naturwissenschaften
der Brandenburgischen Technischen Universität Cottbus-Senftenberg
zur Erlangung des akademischen Grades eines
doctor rerum naturalium

genehmigte Dissertation
vorgelegt von

Master of Science in Agriculture
Annika Badorreck
aus Rendsburg

Gutachter: Prof. Dr. rer. nat. habil. Dr. h.c. Reinhard F. Hüttl
Gutachter: PD Dr. Horst H. Gerke
Tag der mündlichen Prüfung: 21.11.2016

» ‚Der Übergang vom Affen zum Menschen, das sind wir.‘
Diese Erkenntnis hat uns Konrad Lorenz bereits vor Jahren mit auf den Weg gegeben. Noch haben wir die Möglichkeit, uns zu entscheiden - *und unseren Kindern vorzuleben* -, wo wir eigentlich hinwollen. «

Prof. Dr. Dr. Gerald Hüther
(Neurobiologe, aus der „Bedienungsanleitung für ein menschliches Gehirn“)

Declaration of Originality

I declare herewith, that this dissertation is my own original work, unless stated otherwise.

No other person's work has been used without due acknowledgment in this thesis. All references and verbatim extracts have been quoted, and all sources of information, including graphs and data sets have been specifically acknowledged.

Cottbus, 28.06.2016

Annika Badorreck

Table of Contents

List of Figures

List of Tables

List of Abbreviations

2D	two-dimensional
3D	three-dimensional
CCD	charge coupled device
CT	computed tomography
NR	neutron radiography
NT	neutron tomography
REV	representative elementary volume
WDPT	water drop penetration time

1. Preface

Soil is a thin layer of the earth with a highly complex nature and is dynamically changing by linked abiotic and biotic factors such as climate, vegetation and soil fauna. Owning to the process of these soil forming factors, soils exhibit an inherent degree of locally heterogeneous properties and structures at multiple spatial scales. The soil structure influences processes such as erosion, infiltration, matter dynamics, vegetation establishment (e.g., Bradford et al., 1987; Assouline et al., 2001) and hydrological processes. Hydrologically, soil is an important resource for fresh water – as reservoir and filter system. It transforms discontinuous precipitation into continuous discharge to aquifers and hereby partly retains, transforms and releases substances dissolved in the percolating fluid. However, it is also well documented that chemicals can be transported through soils over long distances and occur in the groundwater a short time after application at the soil surface. Cracks and channels formed by swelling and shrinking, decayed roots or soil fauna provide pathways through which water and solutes can rapidly reach large depths (Beven and Germann, 1982). This phenomenon is called preferential flow or macropore flow. The process of preferential flow is known as rather the rule than the exception in soils and quantitative prediction is difficult because of the spatial as well as temporal variability of these water conducting regions in the soil. Furthermore, measurements are experimentally demanding because of the variable scale of these flow domains, particularly the small spatial extent of highly conductive pore system.

More recently, non-destructive and imaging techniques are being used for the observation of pore structure and infiltration (e.g., Lehmann and Vontobel, 2000; Werth et al., 2010; Hassanein et al., 2006a). While the non-invasive X-ray micro computed tomography (CT) has frequently been utilized for quantification of macropore structures (e.g., Luo et al., 2010), neutron radiation can be used for determining the water distributions in soils. Infiltration patterns as time-series' of two-dimensional (2D) water content distributions during the infiltration could be mapped by using neutron radiography (NR) (Lehmann et al., 2004a, 2006). In a number of experimental studies NR has been proven as a suitable technique to visualize water flow in artificially constructed sand beds with different degrees of

heterogeneity. In this dissertation, both techniques were used to describe preferential pathways as a soil structure with CT and the process of preferential flow of water with NT. For the first time neutron radiation was applied on undisturbed soil cores to visualize water distributions in natural soils on three examples for heterogeneities of different origin.

One objective of the dissertation was to visualize the soil structure and flow pattern in soils with three differently formed pore networks using NR radiography and the NT tomography experiments. As the relatively new NR technique was applied for the first time to undisturbed natural soil samples, extensive adaption, testing and evaluation were made to find suitable experimental setups for the different aims, respectively. Hence, another strong focus of the dissertation laid on the development of methods for using neutron radiography and neutron tomography. This cumulative dissertation is structured so that each of the three conducted studies forms a chapter on its own. This leads to some repetitions of descriptions of material and methods. In this context specific descriptions of materials and methods are repeatedly mentioned.

In a first approach the local heterogeneity and flow of the water in a mine soil were investigated. At the local scale, mine soil represents a typical dual-porosity medium characterized by lignitic or clayey porous fragments that are embedded in a sand-dust matrix (Gerke et al., 2009; Buczko et al., 2005). Effects of heterogeneously-distributed embedded fragments on flow are largely unknown. The hypothesis was that flow in the sand-dust matrix is restricted to a fine network of flow paths.

The second set of experiments focused on infiltration patterns into the young soil of an artificial catchment. As a key process in this early stage we investigated the structural dynamics at the soil surface. Here, the objective was to observe and relate the structural formation of the top soil surface layers with hydraulic properties for three sites in the catchment.

In a last approach we observed the influence of early colonization of soil fauna in the same catchment. The soil structure modifications from ground beetles and moss vegetation and its effect on water flow were visualized with computed tomography and neutron radiography.

2. Flow patterns in locally heterogeneous mine soils

cf. Badorreck et al. (2010)

2.1. Introduction

The ‘small-scale’ or ‘local’ spatial structures as well as the variability of mineral and organic components can crucially affect preferential flow and transport processes in stony, structured, or otherwise heterogeneous soils (e.g., Schulin et al., 1987; Flury et al., 1994; Jasinska et al., 2006). The term ‘local’ is used here to express a smaller spatial scale (i.e., within a representative elementary volume (REV)) as compared to that of the process model for which certain properties are defined (Bear, 1972). A number of averaging techniques and upscaling concepts are under development, (e.g., Vogel and Roth, 2003; Vereecken et al., 2007; Niessner and Helmig, 2007) as well as micro-scale experimental investigations of naturally structured and complex porous systems (e.g., Hallett et al., 2004; Nunan et al., 2006; Smucker et al., 2007; Peth et al., 2008).

A characteristic example for a porous medium with locally heterogeneous properties and structures at multiple spatial scales may be represented by a mine soil (Fig. 1). These soils develop on reclaimed overburden spoil piles that originate, in the Lusatian district in eastern Germany for instance, from open-cast lignite (brown coal) mining operations (e.g., Hüttl and Weber, 2001). The overburden spoil heaps consist of partly-mixed quaternary and tertiary sediments that are heterogeneous at several spatial scales (Gerke, 2006a). Larger-scale heterogeneity is obvious in the form of inclined layers in the subsoil and a horizontal layer separating the 40 cm deep plowed ameliorated topsoil (Fig. 1a). These layered sediment structures are formed depending on mining and dumping technology and reclamation measures (e.g., Buczko and Gerke, 2005). Locally, each of the mine soil ‘layers’ is composed of a coarser-textured mineral soil matrix with varying fractions of lignitic dust and embedded irregularly-shaped and distributed lignitic fragments or other fine-textured clods. Thus, a mine soil may be regarded as a typical dual-porosity medium with immobile (i.e., fragments) and mobile (i.e., the bulk of the sand-dust matrix) pore domains (Gerke, 2006b).

In addition to these largely physical aspects of heterogeneity, the mine soils may be subject to significant geochemical heterogeneity and acid drainage (e.g., Blodau, 2006; Kelln et al., 2007; Malmström et al., 2008). The tertiary overburden sediments may contain considerable amounts of pyritic minerals that are subject to oxidative weathering upon aeration and spoil acidification (Evangelou, 1995). The spatial distribution of these reactive minerals and the differently-acidified sediments is sensitive to long-term predictions of acid mine drainage (e.g., Gerke et al., 1998, 2001). Moreover, the heterogeneity is severely affecting water and solute budgets of forest-reclaimed mine soil ecosystems (Schaaf et al., 1999; Schaaf and Hüttl, 2006). Previous field observations of flow and transport in a lignitic mine soil block using a suction-cell lysimeter revealed finger- or funnel-type preferential flow patterns (Hangen et al., 2004), while preferred flow paths through macropores surrounding rock fragments were reported for another mine soil (Guebert and Gardener, 2001). The sporadically and locally occurring leaching patterns (Hangen et al., 2005) could not be described using standard flow and transport models (Buczko and Gerke, 2006), even with a full consideration of spatially distributed hydraulic properties (Buczko et al., 2001; Buczko and Gerke, 2005).

More detailed multistep flow experiments with mine soil cores showed discrepancies between local pressure head data obtained with miniature tensiometers and core-scale outflow rates (Gerke et al., 2009): The observed rapid drop in water suction upon infiltration did not correspond with the simulated water flow rate. Simulations with a spatially-resolved 3D numerical flow model that considered the local-scale distribution and geometry of lignitic fragments and an equivalent 1D mobile-immobile type dual-porosity model yielded comparable results. However, both models failed to simultaneously describe outflow and suction curves. Simulations using a simplified 1D vertical dual-permeability (two mobile pore domains) model suggested the existence of two interacting mobile pore domains (Gerke et al., 2009). Visual inspection indicated that another relatively narrow continuous pore region for rapid flow could exist in the vicinity and in the more weathered outer parts of the lignitic fragments. However, identification of such pore network and local-scale flow paths in lignitic mine soil as well as descriptions of their hydrological function with visualization techniques are

challenging. Qualitative analyses with dye tracers are strongly hampered by the relatively dark appearance of the lignitic dust and fragments (c.f., Hangen et al., 2004). Moreover, the use of fluorescent dye tracers is restricted due to sorption in coal mine aquifers (Aldous and Smart, 1988).

Without additional dopants (i.e., impurities added to alter optical properties) such as salts (Vinegar and Wellington, 1986), the use of non-destructive methods for simultaneous flow and pore structure observations, such as X-ray, remains limited by low contrast between the phases (Kaestner et al., 2008). Similar to X-rays, neutrons can be utilized to visualize the inner structure of non-translucent porous media since the image of the partly attenuated radiation is used (e.g., Lehmann and Vontobel, 2000). The relatively high attenuation of neutrons by hydrogen can be used to visualize the distribution and quantification of 'light' water (H_2O) in porous materials (e.g., Lehmann et al., 2004a, 2006). Neutron imaging has been applied in engineering science, for instance, to determine the water distribution and changes in porous construction materials (Pleinert et al., 1998; Cnudde et al., 2008; Hassanein et al., 2006a) or wood (Mannes et al., 2006). Recently, this method has also been used to study water flow in sandy material or repacked soil aggregates (Carminati et al., 2007; Vontobel et al., 2008; Schaap et al., 2008) and root water uptake by plants (Menon et al. 2007; Moradi et al., 2009; Conesa et al., 2009).

Water content distributions can be mapped in 2D by neutron radiography (NR) and in 3D as neutron tomography (NT). From 2D NR-time series of propagating infiltration fronts, Deinert et al. (2004) determined the hydraulic conductivity and the dispersion of the wetting front in homogeneous sieved sand. For heterogeneous porous media, NT provides a better spatial resolution to describe, for instance, the hydraulic properties of aggregate contacts (Carminati et al., 2007) or the changes in pore structure during compression tests (Koliji et al., 2008). In other NT applications, the effect of small-scale 3D-spatial variability on water fluxes was visualized and quantified (e.g., Lehmann et al., 2006; Kaestner et al., 2007; Vasin et al. 2008). However, due to the longer duration of the imaging for NT as compared to NR, fast changes in water contents cannot be observed in 3D with the NT technique.

The objective of this study was to improve understanding of flow in mine soils by visualizing flow paths under variably-saturated and steady-state multistep flow conditions by means of NR and NT techniques with H_2O as conservative tracer. The focus was on the characterization of the role of lignitic fragments on flow to analyze the dynamics of infiltration and identify local pore-networks that could represent preferential flow paths. Since previous studies focused on water flows in homogenized or artificial repacked soils, the aim of this study was also to test an experimental setup for analyzing naturally-structured intact samples.

2.2. Materials and Methods

Sites

All samples are from pine forest-reclaimed mine soils of the Lusatian post-lignite mining landscape. The experimental areas “Bärenbrücker Höhe” (BB) (cf., Hangen et al., 2005) and “Domsdorf” (Do) (cf., Schaaf et al., 1999) are located in the vicinity of the city of Cottbus in eastern Germany (i.e., BB: 51°81’N and 14°46’E; Do: 51°58’N and 13°45E). Both coarse-textured mine soils were mainly composed of differently-sized quartz sand with inherent heterogeneity (Table 1).

Table 1. Mean values (3 replicates) and standard deviations (in parentheses) of basic mine soil properties at the sites BBt (Bärenbrücker Höhe, tertiary sediment), BBq (Bärenbrücker Höhe, quaternary sediment), and Do (Domsdorf, tertiary); the sampling depth was 100 - 150 cm.

	Particle size distribution†							
	Sand							
Site	Coarse	Medium	Fine	Silt	Clay	Bulk density	C_{org}‡	pH (H_2O)
	kg kg^{-1}					g cm^{-3}	%	
BBt	0.04 (0.048)	0.06 (0.052)	0.73 (0.098)	0.05 (0.001)	0.08 (0.009)	1.21 (0.045)	2.11 (0.580)	2.77 (0.030)
BBq	0.11 (0.017)	0.43 (0.039)	0.38 (0.052)	0.04 (0.001)	0.02 (0.003)	1.66 (0.053)	0.26 (0.143)	7.00 (0.577)
Domsdorf	0.35 (0.055)	0.40 (0.059)	0.09 (0.051)	0.02 (0.008)	0.07 (0.031)	1.18 (0.172)	1.19 (2.047)	4.33 (0.306)

† Particle size fractions with ranges 2-0.63 mm for sand, 0.63-0.002 mm for silt and <0.002 mm for clay

‡ organic carbon content (Corg) of the fragment-free soil matrix (<2 mm) determined as total carbon with a CNS-analyzer (Vario, Elementar Analysensystem, Hanau, Germany); anorganic carbon was not detectable

At the BB site, two soil pits located about 25 m apart were opened, both ameliorated with power plant ash to a depth of about 40 cm: The soil type of one trench (Fig. 1, left) with tertiary sediments (i.e., BBt), was classified as (hyperhumic, endohyperthionic) epispolic Technosol according to the FAO scheme (WRB, 2006).

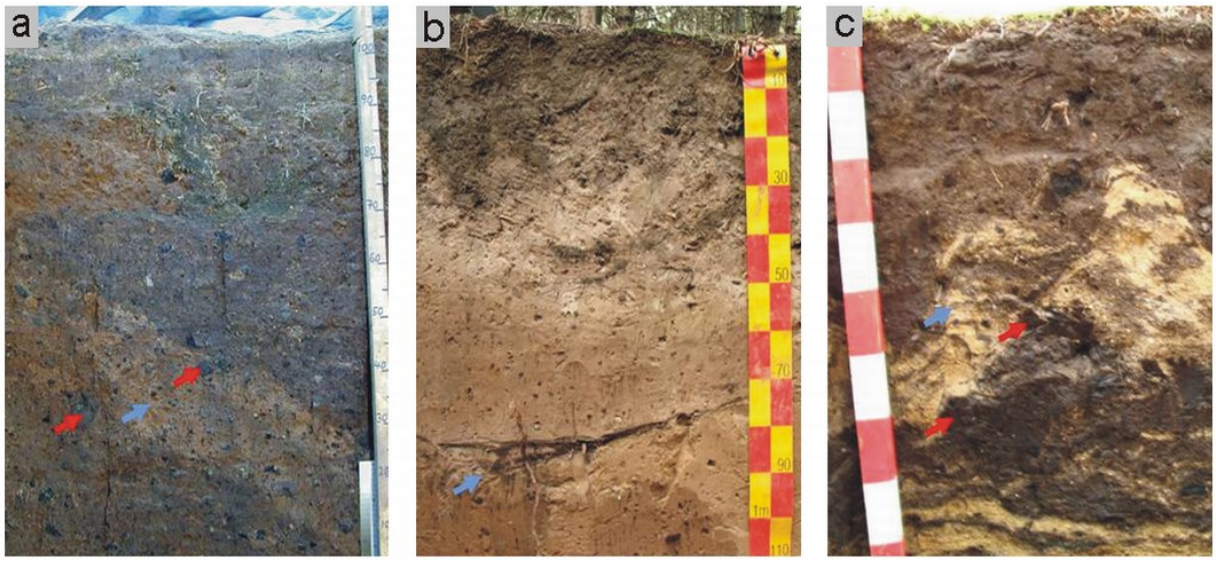

Fig 1. Photographs of mine soil profiles at BBt (a), BBq (b) with depths of 110 cm, and Do (c) with 85 cm; red arrows point at lignitic fragments (black spots), blue arrows indicate dumping structures.

The BBt mine soil consisted mainly of fine sand with varying components of lignitic dust particles and up to about 30 vol.% lignitic fragments. These lignitic fragments had a bulk density of about 1.1 g cm^{-3}, contained about 20% organic carbon and 2% gypsum (Gerke et al., 2009), were of various sizes and shapes and were irregularly distributed within the matrix. The other trench (Fig. 1, centre) was composed of lignite-free quaternary sediments (i.e., BBq) of medium to fine sand (Table 1), and showed a soil type classified as epispolic Technosol (WRB, 2006). The mine soil at the Do site (Fig. 1, right) was classified as (humic, endothionic) epispolic Technosol and was characterized by 20-cm deep power plant ash-ameliorated topsoil; the subsoil consisted of tertiary sediments mixed with lignitic dust-free quaternary sandy sediments. At the Do site, tertiary overburden sediments have been dumped, in contrast to the BB site, with a relatively small-scale technology that created smaller dumping patterns and more loosely structured soil (Fig. 1 centre). The bulk density values were significantly lower and the C-contents higher for soils at the tertiary sites BBt and Do as compared to the soil at BBq because of relatively lighter lignitic components; the corresponding differences in pH-values reflected recent sulphide oxidation in tertiary sediments (Table 1). At all three locations, samples for NR and NT were obtained from soil

depths of about 1 - 1.2 m to avoid possible effects of any admixture of ash or potential compaction from reclamation and amelioration.

Neutron beam facility and theoretical background

We applied thermal neutron radiation at the beam line NEUTRA located at the Paul Scherrer Institute (PSI, Villigen, Switzerland). Here, the radiation is generated through spallation in the neutron source SINQ where the thermal neutron beam is guided and parallelized by a collimator to the experimental station NEUTRA (Lehmann et al., 2004b). For our experiments we used a neutron flux of 5 10^6 [n cm^{-2} s^{-1}] with a collimation ratio (L/D) of 550. The neutrons left the flight tube that had a diameter of 40 cm and were attenuated or scattered by the object to scan or hit the detector behind. A nickel-silver doped scintillator was chosen as neutron detector, which converted the radiation that was transmitted through the sample into light. A cooled slow scan charge coupled device (CCD) camera finally captured the light patterns and yielded gray-scale images. The NR-images were obtained by two camera set-ups each having a different 2D image resolution. The images of sample BBt from measurements in the larger chamber have a spatial pixel resolution of 256 µm. All other 2D time series have a pixel resolution of 147 µm. More technical details of the NEUTRA facility and detector options can be found elsewhere (Lehmann et al., 2004b, 2005; Vontobel et al., 2006).

2D steady flow experiments using NR

For the NR steady state flow experiments at -5 hPa, aluminum slab-type chambers were used that had a thickness of 2 cm and side lengths of 11 cm for the samples from Do and BBq and of 13 cm for those from BBt. For the steady flow experiment at -30 hPa with the sample from BBt, an aluminum chamber of 11 x 9 x 1.5 cm^3 was used. The removable side walls of the chambers of all samples could be locked by screws. The inner walls were coated with a hydrophobic layer of silicone (Dow Corning 1107 fluid, Dow Corning Corporation, Midland, USA) to prevent possible bypass flow along the chamber walls.

The undisturbed samples were collected from each soil pit in three replicates as follows: Because of high coherency of the material, it was possible to manually cut an undisturbed sample-sized soil volume out of the vertical wall of the soil profile by means of a knife. With one larger side-wall removed, the rectangular frame of

the chamber was gently pressed onto the excavated squared soil volume and resized with a knife to obtain an intact central soil slice of 2 cm thickness. Finally, excess soil was removed and the chamber closed. Since the 6 walls of a container were screwed together without any further sealing, small openings remained along all 12 edges of the hydrophobic layer-coated aluminum frame that allowed air exchange with the surrounding. The air-gaps ensured avoiding air entrapment inside the soil samples during the flow experiments.

The detection of infiltrating H_2O within the sample made it necessary to remove the moisture that was initially present in the samples. In order to avoid shrinkage upon drying, initial moisture was removed through exchanging the H_2O in the sample with deuterium oxide (D_2O): D_2O attenuates the neutrons to a far lesser degree than H_2O, while having similar properties except for a 10% higher density. Regarding the terms ‘water’ and ‘soil moisture’, we distinguish in the following between H_2O (i.e., light water) used as tracer and D_2O (i.e., heavy water), which also ‘moistened’ the soil, but was not quantified in our experiments.

The H_2O was gradually exchanged with deuterium oxide (99.8 vol. % D_2O, Chemotrade Leipzig Chemiehandelsgesellschaft GmbH, Leipzig, Germany) while the samples were kept under ‘field moist’ conditions (now with D_2O) to avoid any drying effects on the pore system (e.g., by cracking or shrinkage). In the procedure, one flat wall of the container was removed and the sample fixed in a slantwise position. The D_2O was gently dropped on top of the sample until free D_2O was visible at the sample surface and started exfiltrating at the bottom with a pressure head of -60 hPa through a membrane. After the outflow had ceased, the next D_2O was applied. The procedure was repeated two times.

For the experiments, unsaturated steady-state through flow was initiated at -5 hPa (and at -30 hPa at one sample from BBt) using D_2O and a double-membrane construction at top and bottom sides of the samples (Fig. 2a).

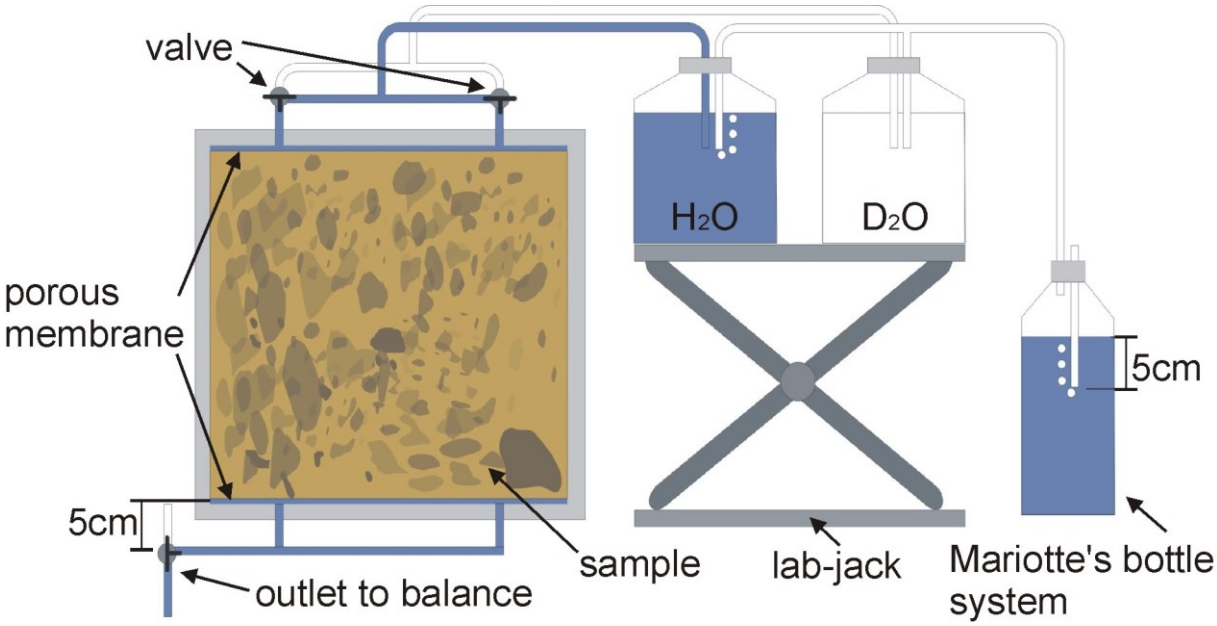

Fig 2a. Sketch of the double-membrane steady-state flow experiments with rectangular slab-type mine soil samples in an aluminum chamber used for 2D neutron radiography.

After steady flow condition with D_2O was achieved, we took a first NR image that served as reference image. The infiltration was then switched to tap water (H_2O) and NR images were taken in intervals between 30 and 60 sec. In addition, the total effluent mass was recorded using a lab scale (Fig. 2a). The density of the effluent was assumed to be 1.1 g cm-3 because the NR images showed that mainly D_2O exfiltrated during the experiments. The experiments were stopped after the propagating H_2O front had reached the bottom of the container and no changes in the H_2O distributions between five following images could be detected (i.e., when a quasi-'equilibrium' state was reached). For the experiment at -30 hPa, equilibrium state could not be achieved and the flow was stopped after 14 h.

Multi-step flow experiments using NT

The intact core samples for the NT experiments were taken by manually pushing aluminum rings of 4 cm inner diameter and 5 cm height in vertical direction gently into the soil while cutting off the excess soil material at the bottom of the core with a knife. The mine soil cores were collected between 1 and 1.1 m depths from soil

pits at BBt. Here, the core samples of 62.8 cm^3 were taken in three replicates. The moisture initially present in the samples was exchanged with D_2O in a slightly different way as described above for slab-type samples. The D_2O was applied at the top of the field moist soil until near-saturated conditions were achieved. The samples were then drained through the bottom on a sand bed with a hanging 'water' column device by applying a pressure head value of -100 hPa while the sample surface was left open for evaporation for 3 days. This saturation and drainage procedure with D_2O was repeated twice before the samples were finally equilibrated at -120 hPa (at the bottom) using a hanging D_2O column.

Before starting the flow experiments, the core samples were NT-scanned in 3D to obtain an image of their internal structure, including the fragment distribution and possible disturbances through sampling. The 3D structure information was used to select the sample that was most suitable for the flow experiment as well as the locations for installing miniature tensiometers. Based on the location of lignitic fragments, one core sample was selected that allowed installation of miniature tensiometers (UPT-8, Umweltanalytische Produkte GmbH, Cottbus, Germany) with minimal disturbances. Two tensiometers were inserted through pre-drilled boreholes from the sample surface. One tensiometer was positioned in the lignitic dust-containing sandy matrix, and the other in the close vicinity of a larger fragment. The core sample including the tensiometers was fixed to a frame (Fig. 2b).

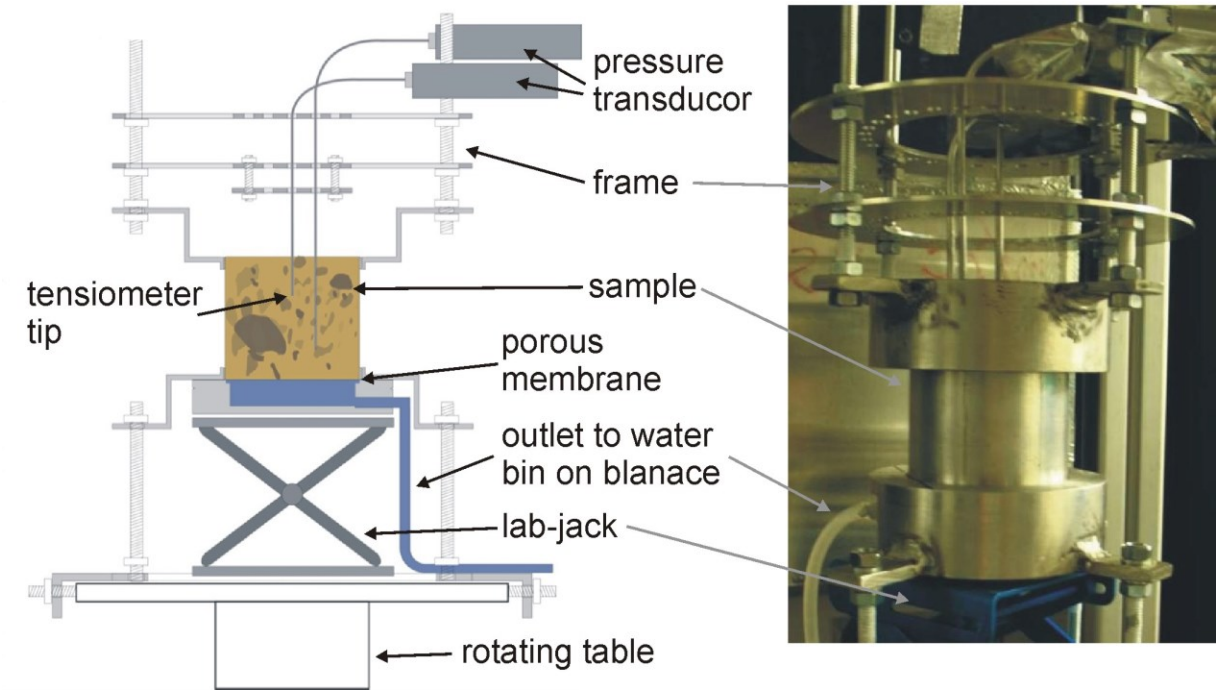

Fig 2b. Sketch (left) and photograph (right) of the multistep flow experiment with cylindrical soil core used for 3D neutron tomography (NT) imaging.

The sample was NT-scanned again for a second time to obtain the initial H_2O-free condition at -120 hPa as a reference. The aluminum core with the sample was positioned in the centre of an aluminum frame on a porous nylon membrane of 10 µm mesh size (HYDRO-BIOS Apparatebau GmbH, Kiel, Germany), and connected to a water storage bottle that was placed on an automatically recording balance for controlling in- and outflow rates. Maintenance and adjustment of pressure heads was controlled by a Mariotte's bottle. To avoid infiltration of water through the membrane into the sample before the start of the experiment, aluminum foil was placed between the sample's bottom and the membrane.

The multistep flow experiment was started by removing the aluminum foil and allowing upward infiltration from the bottom into the sample, initially at -120 hPa to approach by steps the following equilibrium conditions: first with -30 hPa, and then with -15 and -3 hPa. The ex-filtration steps were followed by dropping the water potential from -3 to -15 hPa and then finally to -30 hPa. For infiltration, a mixture of water with deuterium oxide was used (75 vol. % H_2O and 25 vol. % D_2O) to reduce the beam hardening effect and avoid saturation of the detector. The dynamic stage of the infiltration process was visualized by a series of NR scans. An immediate

quantitative analysis of these images made it possible to determine the approaching 'equilibrium' stage, defined as a situation of negligibly small changes in the division of the latest radiography by the antecedent one (i.e., result of 1 over at least 15 min). At each 'equilibrium' step, the sample was NT-scanned to obtain the 3D spatial distribution of infiltrated water at the respective equilibrium stage.

Image processing and H2O content calculation

The captured 16-bit gray-scale images were used for the time-resolved quantification of H_2O contents of the 2D and 3D experiments. Such a radiographic image $I(x,y)$ [L^{-2} T^{-1}] can be regarded as a 2D expression of the reduced neutron flux of the incident beam $I_0(x,y)$ [L^{-2} T^{-1}] described by Beer's law of attenuation (Lehmann et al., 2004a) as

$$I(x,y) = I_0 \cdot e^{-\Sigma(x,y)\cdot d(x,y)} \quad [1]$$

where Σ [L^{-1}] is the total linear attenuation coefficient (or macroscopic cross-section) of the scanned material with the thickness d [L]. The ratio $I(x,y)/I_0(x,y)$ is called the transmission. The coefficient Σ [L^{-1}] summarizes the individual attenuation coefficients of each contained element in beam direction, for the 2D flow experiments we get for each pixel (adapted from Moradi et al., 2009):

$$\sum(x,y) = \sum Soil(x,y) + \sum Al(x,y) + \sum H_2O(x,y) + \sum D_2O(x,y) = ln\left(\frac{I_0}{I}\right)\Big/ d \quad [2]$$

with the components Soil, which is the dry solid soil (i.e., mostly quartz and lignite), Al is the aluminum of the frame, H_2O is infiltrating light water, and D_2O is heavy water present in the sample. This interaction probability between the neutron radiation and the material is known for every element. Neutrons are effectively attenuated by light materials like hydrogen expressed in a high attenuation coefficient of 3.48 [cm^{-1}] for H_2O (Lehmann and Vontobel, 2000), compared to other soil components like quartz sand with 0.25 (Vontobel et al., 2008), and wood with 0.58 [cm^{-1}], while heavy water has a coefficient about 0.4 [cm^{-1}] (Lehmann and Vontobel, 2000).

The processing of the transmission NR-images taken by the CCD camera comprised first the subtraction of a dark current image from the raw image to compensate for the dark current of the CCD chip. Secondly, white spots of a few pixels widths were eliminated with a median filter (3 x 3 pixels, 5% threshold). These spots are usually produced when gamma rays created by neutron capture in the sample material or detector, hit directly the CCD chip. Thirdly, a subsequent flat-field correction was applied to account for spatial heterogeneities of beam intensity and detector sensitivity. Temporal fluctuations in beam intensity were also compensated by normalization. Since the H_2O in the sample scatters rather than attenuates the neutron radiation, a correction for sample scattering and spectral effects was performed.

We used a reference image of the samples, taken as the steady state flow with D_2O was reached and just before the infiltration of H_2O. The reference image was subtracted from each of the time series' images, that the calculation of the H_2O thickness in beam direction *d* (Eq. [1]) and subsequent the volumetric H_2O content was possible, by taking the soil slab thickness into account. All image corrections and finally the quantification of H_2O were carried out using the algorithm included in the computer program Quantitative Neutron Imaging (QNI, Version 1.0) developed by Hassanein et al. (2005). For additional information about the scatter correction, the reader is referenced to Hassanein et al. (2005) and Hassanein (2006b).

For the NT-imaging, the core sample was rotated in 306 angular steps totaling 180˚. At each step (i.e., a projection), an image was taken. A mathematical reconstruction from all projections with the images generated a 3D tomographic representation of the sample volume using the fast filtered back transform algorithm GridRec (Dowd et al., 1999 cited from Kaestner et. al., 2007) available within the PSI reconstruction software.

2.3. Results

Neutron radiography time series

From the initially water-free 2D radiographs an inner structure of the samples was clearly visible, although the ‘structure’ here was probably based on the different physical and chemical properties of the components. The time-series of NR images during unsaturated steady-state flow conditions at -5 hPa (Fig. 3) for all three mine soils and at -30 hPa for BBt only (Fig. 4) illustrate characteristic 2D H_2O content distributions depending on internal structures, distribution of sediment properties, and water-filled porosity.

The water-free radiograph of the sample BBt (Fig. 3a, a.1), captured before the infiltration, revealed the inner structure with lignitic fragments, distinguishable through the relatively low transmission between 0.05 and 0.3, while the sand-dust matrix showed a transmission more than 0.4. The large fragment itself revealed some heterogeneity including several cracks. For the BBt sample (Fig. 3, a.2-5), the H_2O front was initially relatively homogeneous while later, it became more dispersed. The larger lignitic fragment in the central part attracted more water than the immediate surroundings; highest H_2O contents (<50 %) were found in some surface-near fragments. The integrated 1D vertical H_2O content profiles shifted from a typical infiltration-type towards a linearly decreasing depth function.

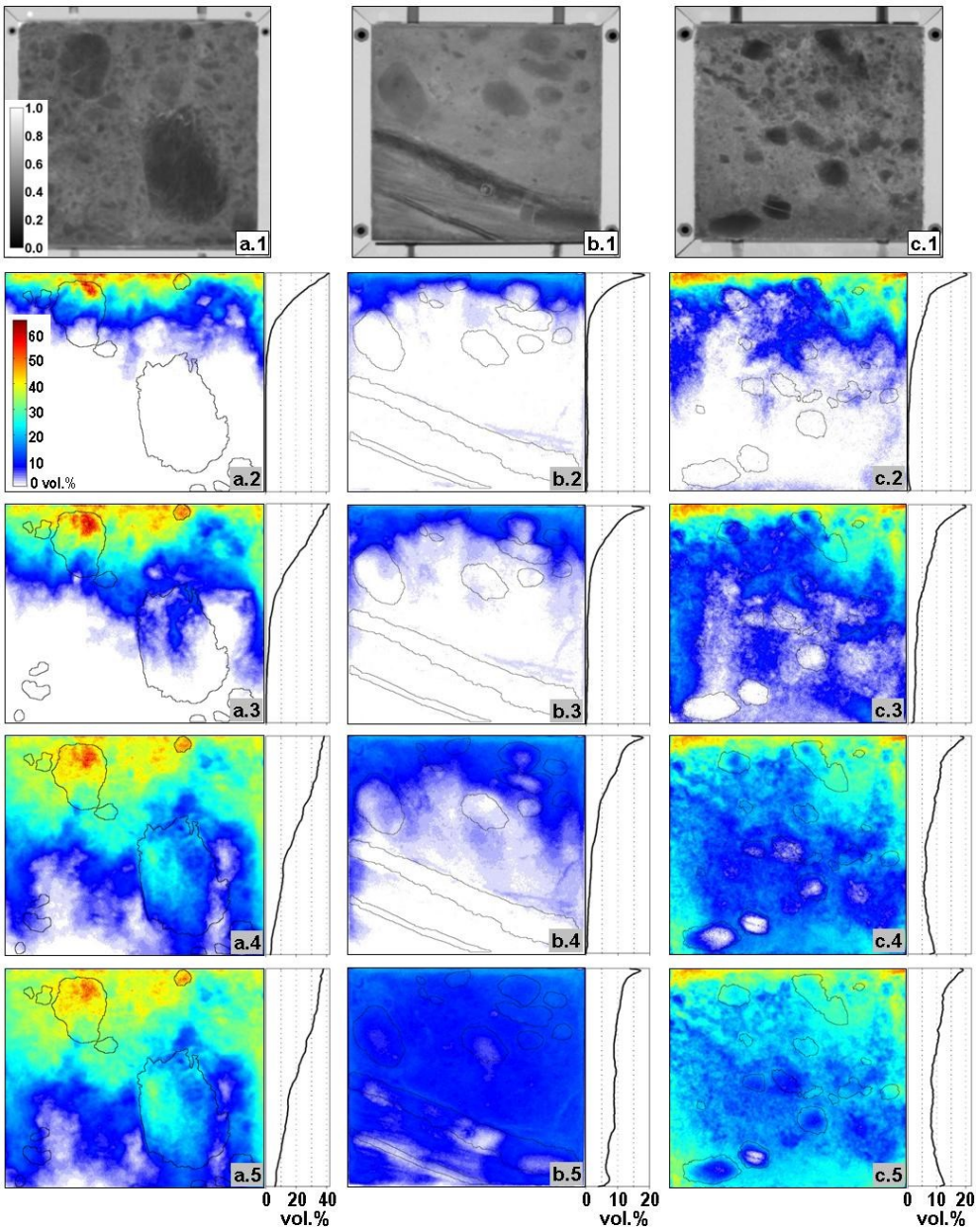

Fig 3. Neutron radiography (NR) dimensionless transmission images of initially H_2O-free samples (first line of the pictures, scale bar left) from (a) the tertiary (BBt), (b) the quaternary Bärenbrück site (BBq), and (c) the Domsdorf site; and 2D volumetric H_2O content distributions (color scale upper left) during steady-state flow at -5 hPa at 15 (2^{nd} line), 30 (3^{rd}), and 60 min (4^{th}) and at the end (5^{th} line) after 82 (BBt), 248 (BBq), and 110 (Do) min after infiltration with H_2O; red arrows at c.1 and c.4 indicate a cracked lignitic fragment. The horizontally-integrated water content profiles are given at the right side of each color image.

The water-free radiograph of the BBq sample (Fig. 3, b.1), which was lignite-free, had a generally higher transmission, with the exception of the inclined layer in the bottom part consisting of organic matter. The infiltration took place at significantly lower H_2O content values (<20 %). Flow was relatively homogeneously distributed within the sandy matrix, while the finer-textured fragments were initially bypassed, and later the fragment H_2O contents were gradually increasing. The inclined layers acted as a slight barrier such that some regions underneath the layers remained almost H_2O-free until the end of the experiment (Fig. 3, bottom). The final 1D H_2O content profile is nearly approaching the theoretically expected uniform moisture distribution for steady flow, here at about 10 vol.%.

The initial transmission image of the coarser-textured Do sample (Fig. 3, c.1) also clearly showed more homogeneously-distributed lignitic fragments and an inclined material boundary crossing diagonally through the central part. The matrix of the upper left part with a lower transmission consisted of a sand-dust mixture, the lower left part of lignite-free sand. The sample showed the most heterogeneous flow patterns of the three soils. Here, in contrast to the BBt sample, the lignitic fragments were initially mostly bypassed, while the flow inside the sandy matrix initially formed finger-like structures (Fig. 3, c.2-3). The integrated H_2O profile was approaching a uniform vertical distribution at values of about 10 vol.% as for BBq (Fig. 3, c.5). However, the increasing H_2O content at the sample bottom indicated effects of a hydraulic resistance at the outlet boundary. Note that the cracked fragment indicated by the arrows remained H_2O-free except for the crack.

For the steady flow experiment with the BBt sample at -30 hPa (Fig. 4), a slightly thinner aluminum container was used (i.e., 1.5 cm in contrast to 2 cm for the other experiments).

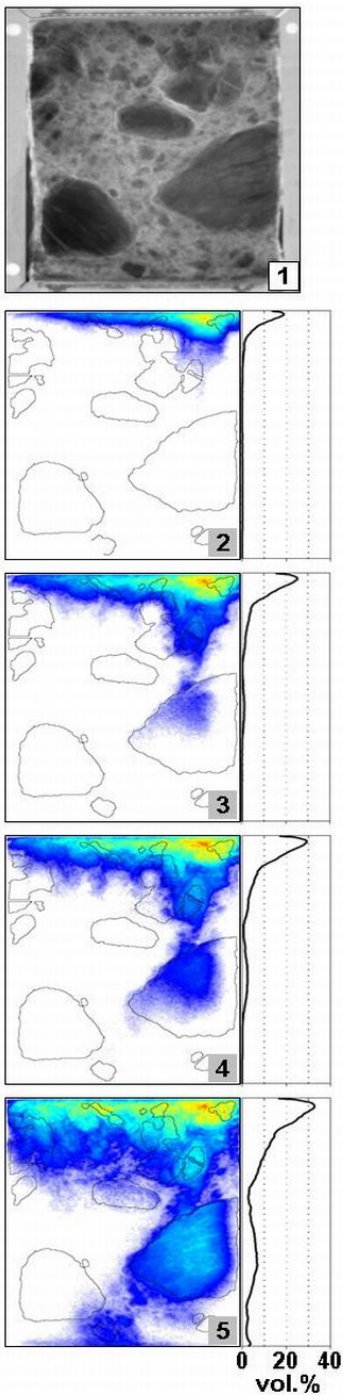

Fig 4. Neutron radiography (NR) transmission image (1) and H_2O content distributions of the sample from BBt for steady-flow at -30 hPa at 150 (2), 285 (3), 390 (4), and 840 (5) min after beginning of infiltration (scale bars are in Fig. 3a); horizontally-integrated NR-derived H_2O content profiles are at the right side of each color image; the red arrows (4) and (5) indicate the location of a hump.

Comparison between the H_2O-free images of both BBt samples (Figs. 3a.1 and 4 top) shows a higher transmission for the thinner sample. The inner structure of the samples matched each other, since the contained larger lignitic fragments indicate a similar heterogeneous appearance. The steady infiltration at -30 hPa yielded more heterogeneous H_2O distributions than the experiments at -5 hPa (Fig. 3). The images for infiltration at -30 hPa (Fig. 4) clearly show a preferential propagation of water near the larger lignitic fragments. The integrated 1D H_2O content profiles developed a hump in the bottom part (red arrows in Fig. 4), although at significantly smaller water contents as compared to the -5 hPa experiment (Fig. 3).

For the 2D steady-state flow experiments, the cumulative outflow volume, V_{out} (t), was measured as mass M_{out} with a laboratory scale and transformed using a density of 1.1 g cm^{-3} at times, t. This is compared with the total volumetric H_2O content in the soil samples, $\theta_{NR}(t)$, obtained from NR-images, calculated as sum of H_2O volume of each pixel over the sample area and taking the sample thickness into account (Fig. 5). As expected from the steady flow experimental conditions, the linearly increasing graphs of measured V_{out} data show that flow rates of 1.88 ml min^{-1} (BBt sample) and 0,98 ml min^{-1} (Do sample) are constant in time (Fig. 5, outflow) (i.e., $V_{out} = V_{in}$). Note that the outflow data are missing for the BBq experiment because of a defect. The curves of H_2O volume obtained from NR-images, $\theta_{NR}(t)$, (Fig. 5, image) reflect the displacement of D_2O by H_2O within the sample volume.

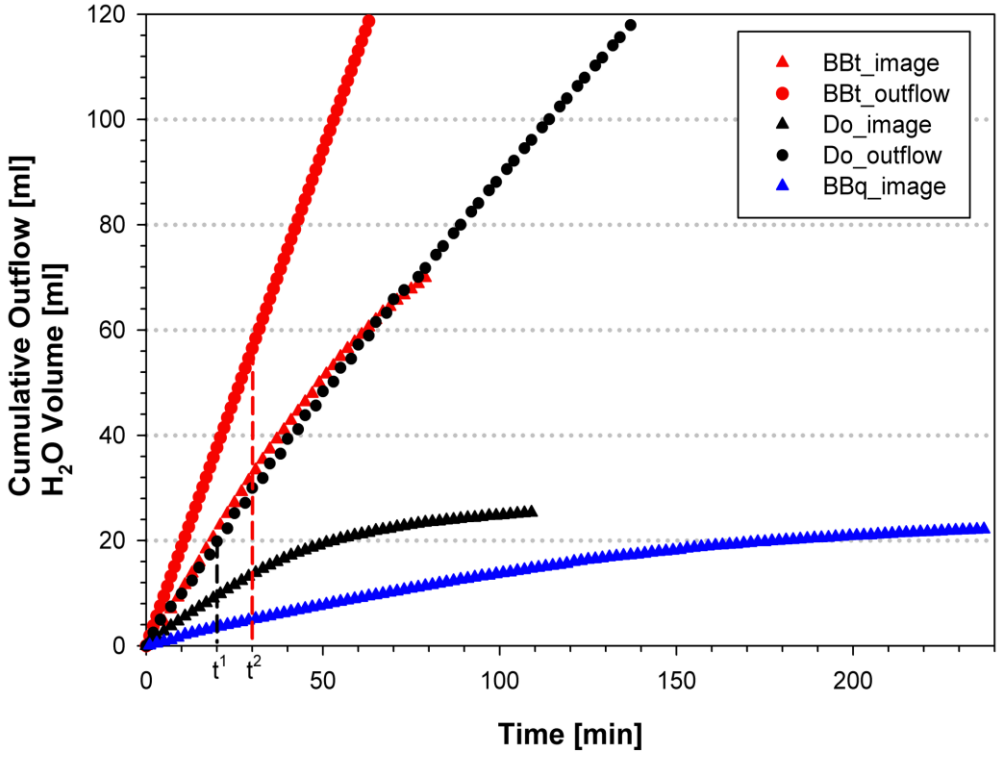

Fig 5. Cumulative outflow volume as recorded by the laboratory scale and the total H_2O volume in the sample as calculated from the NR time-series' images for BBt, BBq and Do. For the BBq experiment, the outflow values are missing because of a failure of the lab scale. The times, t^1 for Do and t^2 for BBt, indicate first arrival of percolating H_2O at the bottom of samples.

When balancing the boundary fluxes with the changes in H_2O volume, $\Delta\theta_{NR}$, two situations can be distinguished. Initially, after starting the experiment by switching to percolation with H_2O (i.e., time t_0), the increase of θ_{NR}, in the sample should be identical with the cumulative outflow (or inflow) volume of H_2O as

$$V_{out}(t)-V_{out}(t_0)=V_{in}(t)-V_{in}(t_0)=\theta_{NR}(t)-\theta_{NR}(t_0). \quad [3]$$

This volume balance equation [3] holds until H_2O hits the bottom of the sample at times, t^* (Fig. 5, vertical lines). Furthermore, for $t < t^*$, the outflow can be assumed to consist only of D_2O. Later, for $t > t^*$, percolating H_2O begins to drain together with D_2O; and eventually, the H_2O volume, θ_{NR}, in the sample will gradually approach a constant value (i.e., $\Delta\theta_{NR}/\Delta t = 0$ for $t\rightarrow\infty$) that is in equilibrium with the steady flow rate as

$$\theta_{NR}(t)=\text{const}. \quad [4]$$

Since the experiments were stopped soon after H_2O reached the sample bottom, the NR-image curves in Figure 5 largely show the linearly increasing $\theta_{NR}(t)$ initial values and the beginning of the approach towards constant sample H_2O volumes. The slopes of the linear parts of the NR-image curves (i.e., $\Delta\theta_{NR}/\Delta t$ for $t<t^*$) are 1.08 ml min^{-1} (BBt), 0.49 ml min^{-1} (Do), and 0.18 ml min^{-1} (BBq).

The rates obtained from evaluation of the NR-images are all smaller than those of the corresponding outflow rates measured with a lab scale (see above). A quantitative comparison for the initial period linear periods in Figure 5 shows that the H_2O volumes derived from evaluating NR images are only about 57 % (BBt) and 50 % (Do sample) of the volumes measured in the outflow. For the period thereafter, the shape of the NR-image curves relate to the unsaturated transport process of H_2O in the samples including mixing of D_2O with H_2O, which is beyond the scope of this study.

Neutron tomography of multistep flow experiment

In the cylindrical soil sample from BBt, two miniature tensiometers were installed in the sandy matrix and near a larger lignitic fragment (Fig. 6).

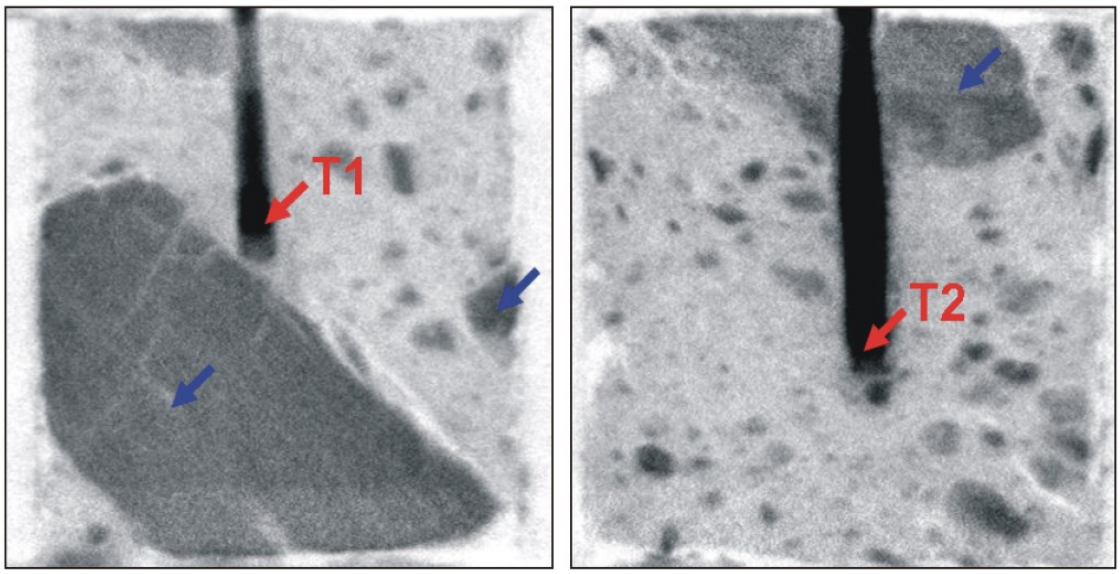

Fig 6. Two vertical cross-sections (4 cm width and 4 cm height) from a neutron tomography (NT) of the BBt mine soil core with lignitic fragments (dark, with blue arrows) and the location of the miniature tensiometers (red arrows; T1 (left) and T2 (right)). The ceramic tips of the tensiometers are in 2.1 cm (T1) and 1.3 cm (T2) height for the bottom.

The tensiometric pressure head data (Fig. 7) indicated a relatively small but distinct local non-equilibrium at short distances during the transient flow conditions at the steps -120 to -30 hPa and close to saturation. Tensiometer 1 in the vicinity of a lignitic fragment increased slightly more slowly from -120 to -30 hPa, but reacted faster at the infiltration step from -15 to -3 hPa. This reverse reaction could be due to a network of larger pores around the fragment, which were more conductive at higher water saturation. The in/outflow curves (Fig. 7) revealed that H_2O uptake of the sample during increasing pressure heads is much larger than the drainage during the following decreasing pressure steps, indicating a hysteretic behavior. Because of a malfunction of the balance, H_2O content (Fig. 7) was obtained from the image analyses.

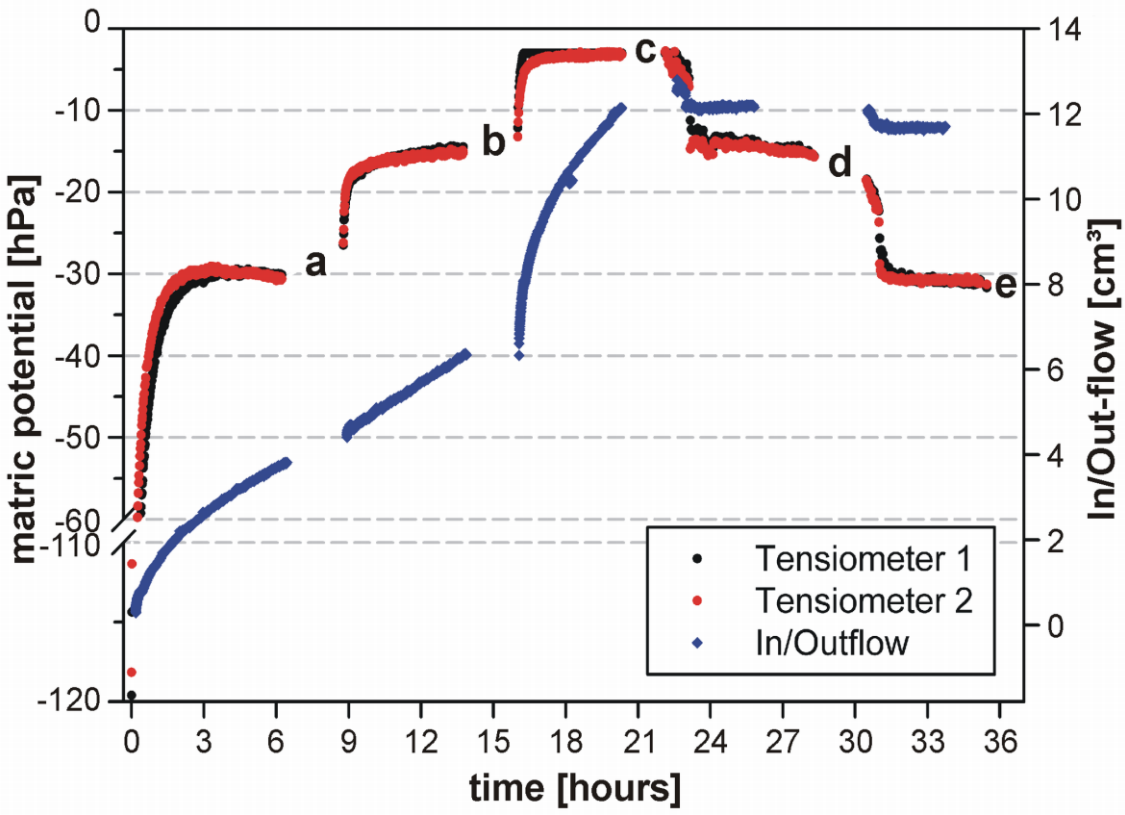

Fig 7. Matric potentials measured with mini-tensiometers and in- and outflow of H_2O obtained from neutron tomography (NT) image analyses as a function of time for the soil core from BBt; the letters 'a' to 'e' indicate relatively stationary phases were tomographies were obtained (depicted in Fig. 6).

Note that these inflow curves still had a tendency to further increase at the end of each pressure step, although both tensiometers already indicated local equilibrium conditions. The relative H_2O content distributions within the core sample for this experiment (Fig. 8) showed that the water is mostly remaining within the pore volume in the regions surrounding the lignitic fragment; however, some water had gradually diffused inside the fragment. The tip of the mini-tensiometer seemed to be connected with the pore regions of higher relative H_2O contents that could have acted as flow paths, especially during near-saturated conditions (Fig. 8c).

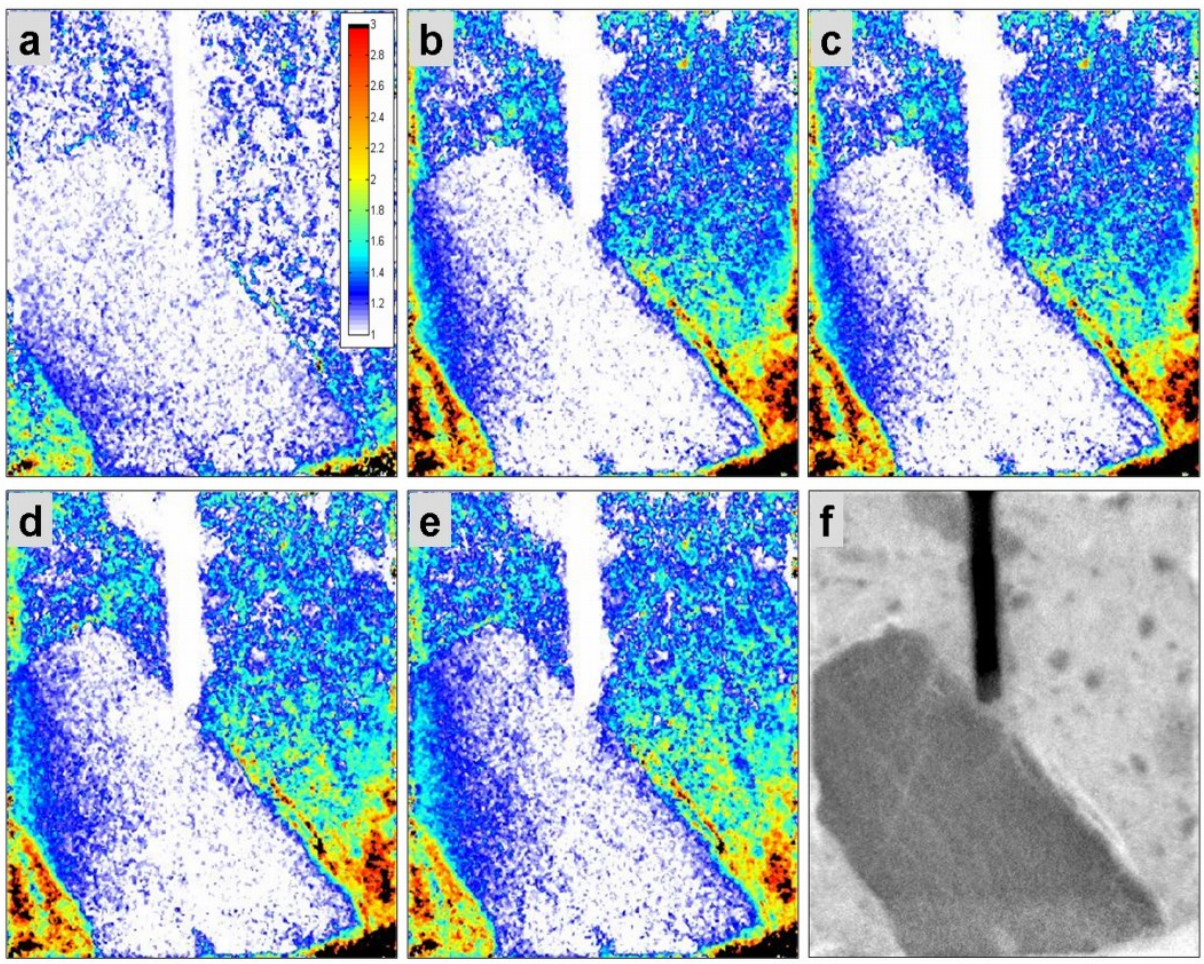

Fig 8. Vertical **c**ross-sections (a-e) (3 cm width, 4 cm height) of neutron tomographies indicating relative water content distributions (i.e., image referenced to initial water-free transmission (f)); from 1 (no H_2O) to >3 (high H_2O content); the slices (a) to (e) correspond to the stationary phases at different pressure head steps at -30, -15, -3, -15 and -30 hPa respectively.

2.4. Discussion

H_2O quantification in undisturbed soil samples

The first aim of this study was the testing of an experimental set-up to quantify H_2O distribution patterns in natural, undisturbed or intact soil samples. The full quantification of infiltrating H_2O volume in the samples could not be achieved as demonstrated by the underestimation of flux rates calculated from NR-images of 43 to 50% as compared to measured outflow (Fig. 5) and failed for the tomography sample (Fig. 7). The underestimation of the H_2O volume in the sample appears relatively large as compared to other studies using the same NR-technique (e.g., Hincapié and Germann, 2009), where water infiltration into dry and only 0.5 - 1 cm thick quartz sand samples was studied. In our case, the conditions (i.e., thicker samples, heterogeneous and lignitic soil material, and residual initial moisture) reduced the accuracy of the technique. Quantification was here probably limited by the following problems:

1. Since the sensitivity of neutrons to hydrogen is relatively high, the maximal light water thickness is about 1 cm, a thickness for which the scattering correction approaches its limit due to the statistical noise (Hassanein et al., 2005). The additional neutron attenuation caused by soil components other than water further reduced this threshold value. Therefore, we tried to compensate for excessive attenuation by reducing the sample thickness and by exchanging the initially present H_2O with D_2O, while keeping the soil structure unaffected from cracking and shrinking. The result of this effort is illustrated in the 2D radiographs taken before the infiltration experiment started (Figs. 3 and 4, top). Here the lignitic samples had generally lower transmission than the sandy regions of the sample BBq. This is probably due to the hydrogen that accompanied the lignitic and organic carbon as well as to the carbon itself. A reduction of the sample size for NR to 1.5 cm sample thickness was only possible for the compacted and coherent soil from site BBt for the measurements at 30 hPa, without affecting the original structure. For the 3D NT experiment, the ‘threshold thickness problem’ was even more pronounced. Still, qualitative H_2O distribution patterns could be obtained. Although a mixture of 25% D_2O and 75% H_2O was used for the multistep

experiment, the initial attenuation of the lignitic fragments was too high for a quantitatively analysis of H_2O contents.

2. Although the exchange procedure before the experiment was carefully conducted and some additional H_2O was washed out during the initialization of steady state flow with D_2O, it was likely to assume that the samples still contained some residual H_2O. Estimation of the amount and distribution of residual H_2O was not possible because any image of a sample in an absolute dry state could not be used as referencing image because of a different pore structure caused by cracking and shrinkage. Two cases (a,b) were distinguished to estimate errors in the H_2O calculation for the 2D experiment:

a. The residual H_2O was immobile during the experiment, because the pores filled with H_2O were separated from the conducting flow pathways in the experiment. This could apply particularly for small pores in lignitic fragments. Immobile H_2O in the sample could be considered as 'background' signal, similar to the soil, and could be also accounted for when subtracting the reference image. An error in the calculation of H_2O was then only possible if the detector was saturated due to low transmission of the reference image. In the subsequent image the additional infiltrating H_2O would be underestimated in this case.

b. The residual H_2O was mobile during the experiment. In this case, the H_2O would have been detected in the beginning of the experiment in the central and bottom parts of the container, before the infiltrating H_2O front reached this region. No such patterns, however, were observed. It was likely that the mobile fractions of H_2O in the lager pores were washed out during the initialization of steady state flow with D_2O.

3. The reference images contained D_2O which was displaced by H_2O during the infiltration. Although the attenuation coefficient of D_2O (0.4 cm^{-1}) is much lower than the one for H_2O (3.48 cm^{-1}), the displacement could lead to an underestimation of the H_2O content. According to the pore size distributions, the D_2O content was assumed to be higher in lignitic fragments than in the surrounding soil matrix, and thus was heterogeneously distributed in the sample. Under steady state flow conditions with local equilibrium in pressure heads, the

water content distributions of both D_2O and H_2O remained constant within the sample before and during the 2D experiments. The displacement of D_2O could only be estimated if we assumed that the quantified H_2O (although underestimated) replaced the same amount of D_2O, what is in the 2D experiment reasonable. The quantity of D_2O and the attenuation coefficient is then known; a transmission image with D_2O can be calculated and subtracted from the H_2O contained image. The correction is not possible for the tomography images because it is not possible to determine if the infiltrating H_2O replace D_2O or air.

4. Another difficulty was the mixing between H_2O and D_2O through molecular diffusion. This could be the case for regions where long time is needed to approach local equilibrium conditions between H_2O and D_2O concentrations as in the 3D experiment. This effect is visible in Figs. 8 d-e, where H_2O continued to enter the fragments although the imposed global water potential was decreased.

Observation of flow paths

The three soil samples selected for the 2D steady state infiltration experiments differed with respect to the distribution, the geometry, and the inner structure of fragments as well as in the content of lignitic dust of the surrounded matrix. The 2D radiography time sequences indicated that flow paths developed according to the sediment heterogeneity and moisture contents. The flow patterns obtained from the BBt samples at -5 hPa and -30 hPa suggested preferential flow paths, particularly within the close vicinity of larger lignitic fragments. The visualized flow pathways were rather pore regions of preferential flow located in the contact zone between the fragments and the surrounding sandy matrix than individual pores or cracks. This contact zone includes also the outer regions of fragments and its pore system differs depending on the structure of fragment and matrix.

Moreover, the experiment at -30 hPa suggested that a network-like porous system existed between the fragments. The initial radiographs revealed that these lignitic fragments had an internal heterogeneity due to cracks, possibly resulting from earlier shrinkage as observed on fragments in the field. Drying of field moist lignitic fragments could potentially cause a volume reduction up to 1/3, accompanied by the formation of meso- and macropores (Androutsopoulos and Linardos, 1986).

While fragments were shrinking, the more coherent matrix of the BBt samples may have allowed the formation of a secondary, more continuous pore network persisting between dried fragments and bulk matrix. For a different mine soil, Guebert and Gardner (2001) explained the development of observed macropores between and next to fragments larger than 1 cm with seasonal wet/dry and freeze/thaw cycles. Although their observation was based on a lignite-free soil, the mechanism could also apply to other mine soils with embedded fragments with a hydro-mechanical behavior that differs greatly from that of the compacted matrix.

The hydraulic effect of such a secondary pore network on the local pressure heads was relatively less pronounced here probably because only relatively small local non-equilibrium developed between regions next to the fragment and the matrix. Nevertheless, the H_2O distribution patterns confirmed the accumulation of water preferably in the pore regions close to fragments. Here, regions at the bottom of the sample (probably of smaller bulk density) may have acted as preferential pathways. The H_2O contents did not change much in the upper parts of the core sample during infiltration indicating that exchange between D_2O and H_2O was limited here.

The initial NR of the sample from Do showed smaller-sized and more homogeneously-distributed lignitic fragments. The flow tended to form finger-like patterns and fragments were bypassed in a less distinctive manner than for the BBt samples. A more continues pore-network could not be observed at -5 hPa. Since the soil depth was identical for all samples, any climatic preposition for cracking could be considered as similar. The major differences, and probably the main reason for the absence of a secondary crack network in the Do matrix were caused by the coarser-textured sediments at Do and the absence of any compaction because of the different dumping technique. A more continuous macropore network through shrinkage of fragments and within the matrix was inhibited by the loose soil structure at Do where preferential flow could only be visualized through a single cracked fragment (Fig. 3, right). For the soil from the lignitic fragment-free site BBq, the silt-clay mineral fragments absorbed water relatively slowly but constantly (Fig. 3, centre). The organic-rich inclined layer in the lower part acted initially as a barrier, but became permeable with ongoing

infiltration. The final H_2O distribution showed a remarkable homogeneity, which is probably characteristic for the lignite-free sandy matrix at that scale.

2.5. Conclusions

Both the NR radiography and the NT tomography experiments could be used to observe highly heterogeneous flow patterns in lignitic mine soils, depending on the structure and the distribution of fragments and moisture contents. The 2D NR time series revealed a secondary higher conductive pore-network in a mine soil with cracked lignitic fragments embedded in a compacted sand-dust matrix. The NR technique was found useful for quantification of light water in soil samples, although with limitations due to sample size and carbon content that could strongly affect background attenuation.

The results suggest that macroscopic flow takes place in the sand/dust matrix and mostly not in lignitic fragments, thus confirming the mobile-immobile hypothesis. However, finger-like flow pathways may develop within the sandy matrix itself. Under near-saturated conditions, water preferably flows around lignitic fragments and within a more continuous pore network of the lignitic dust-containing sandy matrix. The separate consideration of pore regions around fragments and finer-textured local structures may provide a key for improving flow description in soils with similar small-scale internal heterogeneity. Neutron imaging proved to be useful also for heterogeneous soils, although H_2O quantification was limited by detector saturation due to residual water and lignitic carbon contents.

3. Morphology of physical soil crusts and its effect on infiltration patterns in an artificial catchment

cf. Badorreck et al. (2013)

3.1. Introduction

The soil structure of the first centimeters of a soil largely influences many interlinked ecological processes like matter dynamics, vegetation establishment and soil biota (e.g. Six et al., 2004). The associated hydraulic properties of the soil surface control the partitioning of rainfall between infiltration and runoff. One common alteration of bare soils is the formation of a structural surface seal due to the kinetic energy of raindrops during rainstorms. Structural surface sealing occurs during rainfall events when raindrops directly impact the surface and lead to a destruction of aggregates. Further, splashing and detachment of soil particles rearrange in a denser, relatively thin skin at the surface. The following drying period strengthen the seal to a hard soil layer. In this paper we use the term “seal” for the initial wet phase of the surface layer and “crust” for the subsequent dry phase (Romkens, 1979).

The degree of soil sealing depends on many factors, such as energy and intensity of rain, soil properties and slope angle (Mohamed and Kohl, 1987; Assouline and Mualem, 2000; Ribolzi et al., 2011). During the past decades a wide range of involved soil characteristics has been identified such as soil texture and mineralogy, aggregate size and strength, chemical properties affecting the aggregation like the content of organic carbon, gypsum and exchangeable Na (ESP). Also the initial water content, matric potential and water table elevation influences the degree of sealing (Augeard et al., 2007). Moreover the infiltration through seals shows a highly dynamic behavior during rainfall events and depends on the heterogeneity of the hydraulic characteristics (Assouline and Mualem, 2002). An extensive overview of processes and factors involved in rainfall-induced soil sealing as well as conceptual models is given in Assouline (2004). The crust morphology has been described in 2D using thin-section observation (e.g. Valentin and Bresson, 1992; Bresson and Cadot 1992) and more recently in 3D using X-ray tomography (Augeard et al., 2007; Lee et al. 2007). The various processes and causes influencing the genesis of soil seals are reflected in the morphology of their

resulting crusts (Bresson and Boiffin, 1990). Therefore, rainfall-induced surface layers can be divided in two categories, namely the (i) structural crusts, which are formed by slumping and slaking due to the raindrop impact, and (ii) the depositional crusts formed of lateral transported and deposed fine soil particles (Chen et al., 1980). Valentin and Bresson (1992) further characterized and classified sub-groups based on morphology and physical features. They divided structural crusts according to their genesis in categories of slaking, infilling, coalescing and sieving crusts. The depositional crusts were divided in runoff, still water, and erosion crusts.

The formation of a dense soil crust at the surface of bare soils e.g. after tillage and seed bed preparation seriously decreases infiltration and thus triggers runoff and erosion. Due to the consequences for the agriculture, soil sealing have mostly been studied focused on bare cultural field and with rather short time scales.

The present study deals with soil crusts developed in bare soils in an area left to undirected ecological succession. An artificial catchment was constructed to study this initial ecosystem development and runoff generation. However, the initial soil structure formation at the surface is highly dynamic and spatially variable such that the knowledge is limited. The objective was to describe (i) micro-morphology and (ii) associated infiltration patterns of the initial structural formation of the soil surface with hydraulic properties three years after the construction.

We used two visualization methods to obtain macropore structure and infiltration patterns of the soil surface. We applied X-ray micro computed tomography (CT) on undisturbed soil samples containing soil surface samples from three bare and differently textured sites within the catchment.

Neutron radiography technique was used to map water content distributions during the infiltration in two dimensions (2D) (Lehmann et al., 2004a) of samples from the same sites. This method provides time resolved quantitative H_2O distributions of infiltration fronts in soil samples, which can be used e.g. to determine hydraulic properties for sieved sand (Deinert et al., 2004) or to visualize flow in mine soil samples (Badorreck et al., 2010) and water flow along beetle burrows (Badorreck et al., 2012). Moreover, miniature infiltrometer experiments were carried out to obtain soil hydraulic properties.

3.2. Materials and Methods

Site

The research site is the artificially created hydrologic catchment area “Chicken Creek” 20 km south of the city Cottbus (Germany), which is left to undirected succession. The approximately 6-ha catchment area was build in 2005 of coarse-textured quaternary sediments and forms a back- and foot-slope that flattens out to a pond. A clay liner of 2-3 m thickness seals the catchment at the bottom. The initial “soil” layer consists of sandy quaternary sediments of approximately 2-3 m thickness that overlaying the clay liner. The sediments of the artificial system are in the very initial stage of soil formation and the soils are classified as Entisol (US-Soil Taxonomy,) or Regosol (World Reference Base for Soils, WRB, 2006). For general information on this catchment the reader is referred to Gerwin et al. (2009, 2011).

The dumping activities during the construction of the catchment area lead to a heterogeneous sediment distribution, such that the catchment can be divided into three sub-areas according to their particle size distribution (Table 2).

Table 2. Soil characteristics of the three sites ‘east’, ‘west’ and ‘lake’ provided by the site monitoring project of the SFB/TRR 38 (Gerwin et al. 2009).

			Particle-size distribution							
			Sand			Silt			Clay	
Soil	$CaCO^3$ content	Organic matter content	coarse	medium	fine	coarse	medium	fine		Texture
	%									
east	0.05	0.16	6.59	49.90	31.50	3.35	1.80	1.81	5.05	sand
west	0.43	1.71	14.27	46.66	17.13	4.51	5.01	3.76	9.67	loamy sand
lake	0.11	0.51	3.57	3.57	67.22	10.37	4.61	1.47	0.13	silty sand

Since the particle size distribution plays a key role for soil structuring and crusting three sampling locations (“east”, “west”, and “lake”) have been selected for investigation of the structural development of surface crusts and their effects on runoff and infiltration (Fig. 9).

Fig. 9. Aerial map of the “chicken creek” catchment (outlined by black line) with installed monitoring equipment, and the location of the sampling sites (numbered green points: (1) east, (2) west and (3) lake. The aerial map was provided by the site monitoring project of the SFB/TRR 38 (Schaaf et al. 2010).

These soils represent the range of textures within the catchment. The particle size distribution in the first 30 cm of the soil varied between the mostly sandy eastern site (i.e., about 5 % clay) and the more loamy western part of the catchment (i.e., approx. 10 % clay). Note that the particle size classes are 2.0 - 0.063 mm for sand, 0.063 - 0.002 mm for silt, and <0.002 mm for clay. In the area next to the pond, an almost clay-free, silty fine sand was found, which was probably an aeolian deposit resulting from wind erosion, which likely occurred in the catchment area (Maurer and Gerke, 2011). The soil from the western part had the highest

carbonate (0.4 %) and organic matter contents (1.7 %) in the first 30 cm, and the soil from the eastern part the lowest values (0.1 and 0.2 %); the sediment next to the pond had a carbonate content of 0.1% and organic matter content of 0.5 %, respectively.

At the time of sampling in August 2008, the three sites were sparsely vegetated. To minimize and exclude the influence of roots on crust soil structure we collected the soil samples for neutron radiography and micro-CT at a distance of at least 30 cm to the nearest plant.

X-ray computed tomography

The soil cores for the CT analyses were collected in 2008 at the three locations (Fig. 2) in three replicates. For sampling acrylic glass cylinder (3.5 cm diameter, 3 cm height) were carefully pressed about two centimeters into the soil surface while removing the excess soil on the sides manually with a knife.

The nine soil cores were then air dried. The internal structure of the soil density was obtained using an X-ray micro-CT-scanner (XTek HMX 225kV, now Nikon Metrology NV, Leuven, Belgium) at the Department of Soil Physics, Helmholtz Centre for Environmental Research (UFZ), Halle (Saale), Germany. The resulting 16-bit grey-scale volumes had a spatial resolution of 0.084 mm. All CT-scans were processed successively in horizontal (Y) direction as two-dimensional (2D) images (ZX-planes) using plug-ins implement in the image processing package ImageJ (Version 1.4, Rasband, 1997–2009). The images were filtered with median and an edge-preserving anisotropic diffusion filter (Tschumperlé and Deriche, 2003) to reduce the noise level.

Neutron radiography NR

We used the NR technique to visualize water infiltration patterns in crusted soil samples. For the NR-measurements we used the neutron radiation facility NEUTRA at the Paul Scherrer Institut (PSI, Villigen, Switzerland) were the neutron radiation was generated through spallation in the neutron source SINQ. The thermal neutron beam was then guided and parallelized by a collimator to the experimental station (Lehmann et al., 2004b), where it hits the soil sample. A cooled slow scan charge coupled device (CCD) camera captured the remaining beam patterns on a detector behind the sample and yielded 16-bit gray-scale

images with a pixel resolution of 147 µm. For more detailed information of the NEUTRA facility and detector options the reader is referred to Lehmann et al. (2004b, 2005) and Vontobel et al. (2006).

We used slab-shaped soil aluminum chambers with removable walls that could encase a 1.5 cm thick, 8 cm wide and 8 cm high undisturbed soil sample. The inner walls of the aluminum were coated with hydrophobic silicone (Dow Corning 1107 fluid, Dow Corning Corporation, Midland, USA) to prevent possible bypass flow between soil sample and wall.

One undisturbed soil sample per site was taken. The coherent soil allowed manual knife-cutting of rectangular intact soil blocks including the soil surface out of a vertical wall from a trench. With the front panel removed, the aluminum container was gently pressed onto the excavated squared soil volume and resized with a knife to isolate an intact soil slice that exactly fits into the chamber of 1 cm thickness. Excess soil was removed and the chamber closed with the aluminum back panel. The aluminum chamber (panels and borders of the frames) were screwed together without any further sealing to allow soil air exchange during the infiltration experiments. The initially present moisture was removed from the samples by drying the samples at 30°C for 3 days.

For the experiment water-free reference images were taken, before the samples in the aluminum chamber were placed underneath a drip irrigation device. It consisted of 8 disposable hypodermic needles (Sterican, 0.4 x 20 mm, B. Braun AG, Melsungen, Germany) with a spacing of 1 cm each (Fig. 2) which are connected to a supply Mariotte's bottle.

The drip irrigation rates for the infiltration experiments were pre-selected in tests with samples of the same initial condition according to the criteria to imitate realistically high rainstorm intensities while preventing ponding and preferential flow along chamber walls. Hence, water was irrigated at average rates of 27.5 mm/h. Neutron-Radiographic images were taken every 13 sec until the infiltration front reached the bottom of the soil slabs and changes in H_2O content distribution between two subsequent images became negligibly small.

Each radiographic image from the time sequences I(x,y) [L^{-2} T^{-1}] yielded a 2D distribution of the reduced neutron flux of the incident beam I_0(x,y) [L^{-2} T^{-1}] described by Beer's law of attenuation (Lehmann et al., 2004a) as

$$I(x,y) = I_0 \cdot e^{-\sum(x,y)\cdot d(x,y)} \quad [5]$$

where d [L] is the thickness of the scanned material and Σ [L^{-1}] its total linear attenuation coefficient which summarizes the individual attenuation coefficients of each contained element and yields in our case for each pixel (adapted from Moradi et al., 2009):

$$\sum(\mathrm{x,\,y}) = \sum Soil(x,y) + \sum Al(x,y) + \sum Water(x,y,t) = \ln\left(\frac{I_0}{I}\right)\Big/ d \quad [6]$$

with the components *Soil*, *Al* (aluminum of the container) and the infiltrating *Water*. The attenuation coefficient is known for every chemical element. Firstly the NR-images were corrected for the dark current of the CCD chip by subtraction of a dark current image. Then the noise was reduced with a median filter (3 x 3 pixels, 5% threshold) and a subsequent flat-field correction was applied to account for heterogeneities of beam intensity and detector sensitivity. Temporal fluctuations in beam intensity were also compensated by normalization. Since the water in the sample scatters rather than attenuates the neutron radiation, also correction for sample scattering and spectral effects was performed.

We used a reference image of the initial water-free condition, taken before the infiltration. The reference image was subtracted from each of the time series' images, that the calculation of the water thickness in beam direction d (Eq. [1]) and volumetric H_2O content was possible. The image processing and quantification of water contents were carried out using the computer program Quantitative Neutron Imaging (QNI, Version 1.0) (Hassanein et al. 2005; Hassanein 2006).

Mini-Infiltrometer-Measurements

An infiltrometer was used to capture the small scale heterogeneity of the infiltration rates at the three locations as described in the radiography experiments. We used a miniature infiltrometer to avoid problems of common disc infiltrometers such as (1) the leveling of the soil surface and to enhance the contact with the disc and (2) the weight of the disc which is applied to the soil surface. Both, the leveling and

the weight of the disc influence the structure of soil crusts. The miniature infiltrometer with a tip diameter of 4 mm was small enough to account for roughness of the soil surface, which made contact sand unnecessary. The tip was also fixed to an adjustable stand to minimize the pressure on the soil surface under the tip. The infiltrometer measurements were performed in four successive steps with applied pressure heads of -15, -10, -5, and -2 hPa (12 replicates at each site). The hydraulic conductivity was obtained from the steady-state infiltration rates (Ankeny et al., 1991).

3.3. Results

The micro-CT-scans revealed initial structural developments of the uppermost soil surface (Fig. 10). The soil structure varies in type and degree of spatial heterogeneity for each of the three locations as well as for the three replicates, although some characteristic differences in crust morphology could be detected.

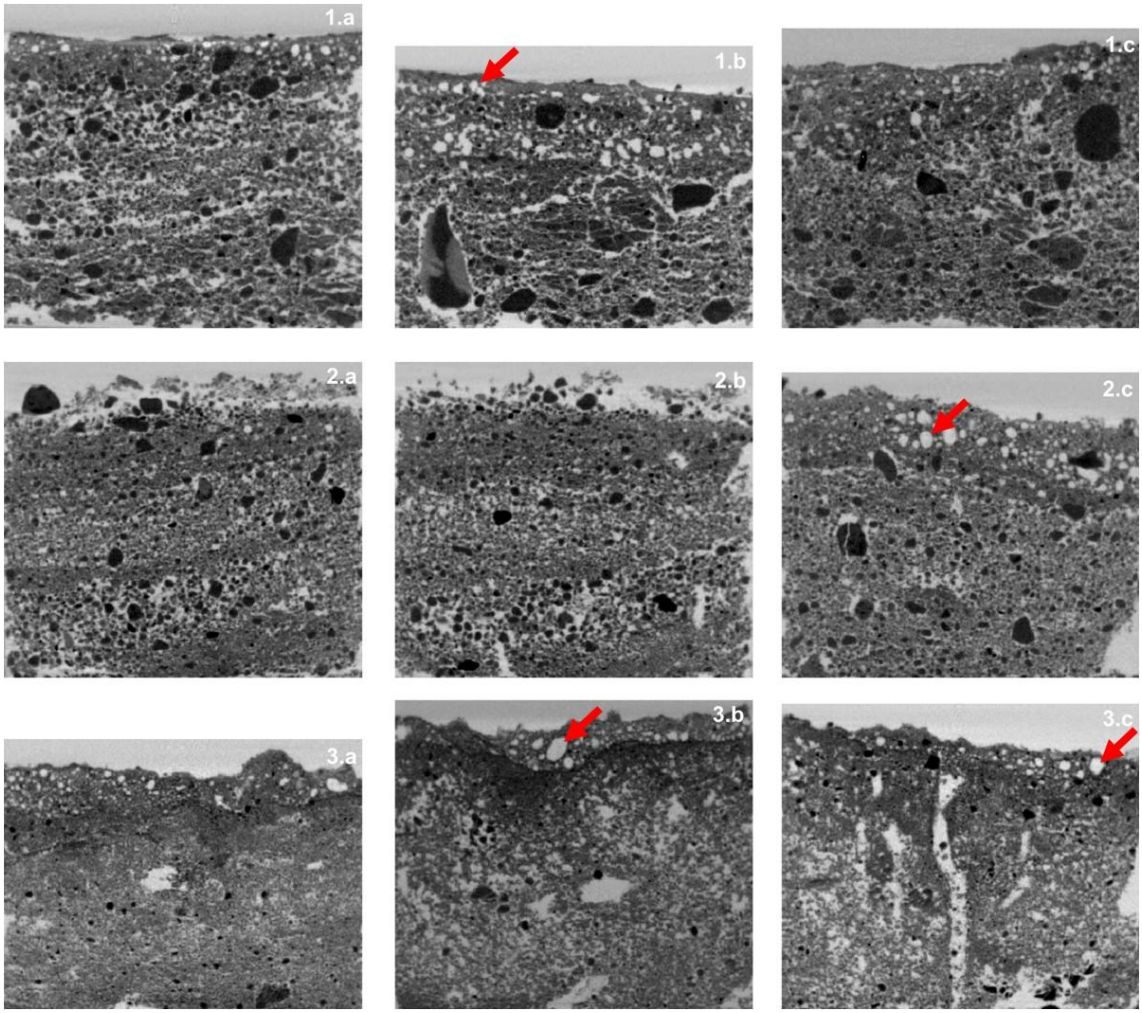

Fig.10. 2D-vertical tomography (CT) slices from the sites 'west' (1.a-1.c), 'east' (2.a-2.c), and 'lake' (3.a-3.c); red arrows point at vesicular pores.

For the samples from the 'west' site (Fig. 10, 1.a-1.c), which is classified as loamy sand with some coarser fragments included, a dense structural crust has been developed with a relatively even soil surface. The soil underneath doesn't show any sign of aggregation or other structural development so far. Within the crust, few round-shaped pores are visible (in the 2D image) that are vesicle-shaped in 3D and appear isolated from the surrounding pore system.

The samples from the ‘east’ site (Fig. 10, 2.a-2.c) show one or several depositional layers, visible by horizontal layers of slightly different density, formed according to the dominating sand-size particles. The soil surface of two samples appears rather rough and diffuse; also vesicle-like pores were absent in this almost pure sand. The third replicate ‘east’ site (Fig. 10, 2.c) differentiates from the other, since the surface appears flat and vesicles could be found in the uppermost layer. A structural development in the bottom part of the three samples was not visible. The samples from the ‘lake’ site (Fig. 10, 3.a-3.c) contained silty to fine sand sediments. The pronounced feature in all replicates was a second depositional crust on top of another structure. The structural crust appears undulating with micro-depressions, which are filled with soil material of lower density and numerous vesicle-shaped pores. In one sample (Fig. 10, 3.c) a vertical beetle burrow is visible that is partly filled with soil particles (see also Badorreck et al., 2012).

Soil slab images (Fig. 11) of the three samples show proceeding infiltration fronts during the first 10 min of the infiltration experiment. The flow in the ‘west’-sample (Fig. 11, 2.a-5.a) seems to be affected by a clayey clod on the left side; here more water is accumulated in the first millimeters of the soil. The infiltration front of the ‘east’-sample (Fig. 11, 2.b-5.b) appears relatively homogeneous and propagates more rapidly as compared to the front in the ‘west’ sample and at a relatively constant velocity. The soil slab from the lake site (Fig. 11, 2.c-5.c) shows isolated water droplets resting on the soil surface. For the ‘lake’ sample, the water free radiograph revealed a layered structure below the surface, which accumulates larger amounts of infiltrating water but does not generally limit the subsequent downward water movement.

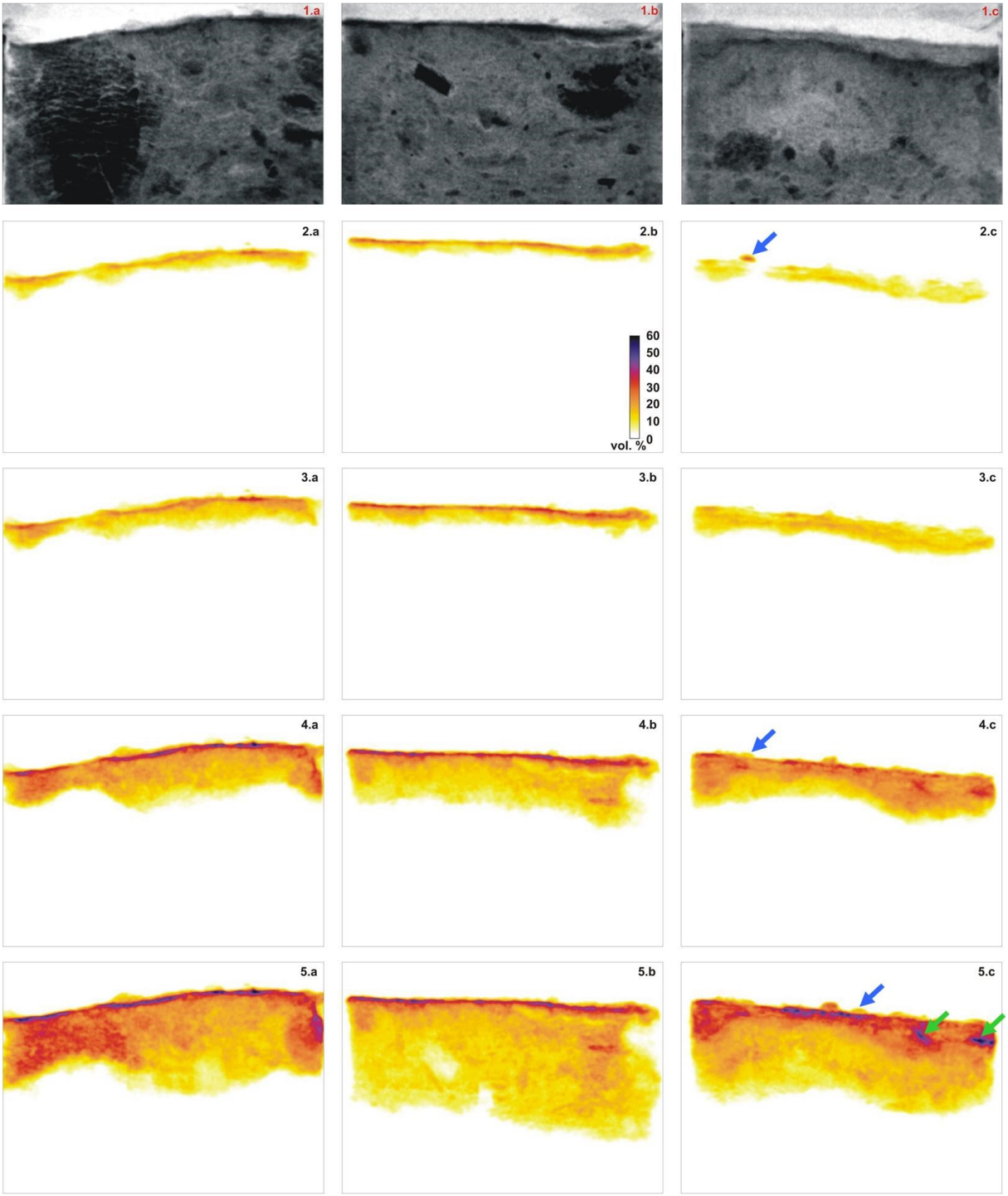

Fig.11. Water free radiographs (1, top series) of soil slabs from 'west' (a), 'east' (b), and 'lake' (c) with 2D (absolute) water content distributions after 1, 2, 5 and 10 minutes (radiographs 2. to 5.) of the infiltration experiment; blue arrows indicate isolated water droplets on the soil surface and green arrows point at location of saturated regions in the soil above the second layered structure.

Measurements using a miniature infiltrometer were conducted in order to determine the unsaturated hydraulic conductivity function of the soil surface layers at the three sites. The infiltrometer-based hydraulic conductivity values at the sites ‘west’ and ‘lake’ (Fig. 12) were relatively similar. No statistically significant difference (Turky test, $P<0.05$) could be identified between these two sites at any pressure step.

The hydraulic conductivity at the site ‘east’ (relatively sandy) was highest in the range from -0.2 to -1 kPa no infiltration was observed at the -1.5 kPa step in eight out of 12 measurements. The hydraulic conductivity was significantly different (Turky test, $P<0.05$) as compared to the values at the other two sites except for the pressure head step at -1 kPa. Here, no difference was detected between the locations.

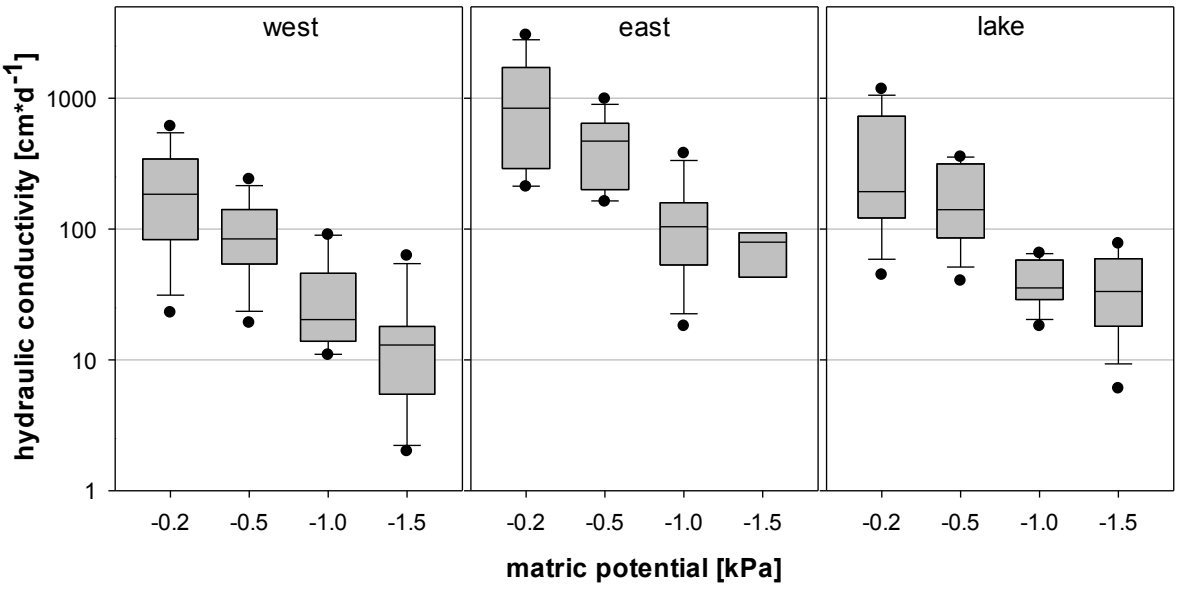

Fig. 12. Unsaturated hydraulic conductivities from miniature infiltrometer measurements as a function of the pressure head for the three investigated sites (12 replicates, for -1.5 kPa pressure step at “east” site only 4 replicates).(The boxes indicate the 25th and 75th percentiles, a line within the box marks the median. Error bars indicate 10th and 90th, points 5th and 95th percentiles.

3.4. Discussion

Morphological crust types

The morphological characteristics of soil crusts can be regarded as a result of variable substrate and mechanisms of formation. Generally two main types of crusts could be found in the chicken creek catchment (Fig. 10) according to the classification from Chen et al. (1980): structural and depositional crusts. Soil structural features (e.g., aggregates or biopores such as root channels or burrows) were generally absent in all soil samples.

The strongest structural soil crust was found in the western part where more loamy sand containing 9.7% clay was deposited (Fig. 11, 1.a-1.c). Here, the impact of raindrops destabilized the bare soil surface, since aggregation had not started so far. Rearrangement of finer soil particles created a seal, which provided the basis for the formation of a soil crust after drying. This crust hampered the infiltration as indicated by the infiltrometer measurements (Fig. 12). The soil crust in the coarse-textured eastern part was of depositional nature (Fig. 11, 2.a-2.c); possibly due to the relatively higher sand content, the slumping effect of raindrops could not take effect. The layered structure in the first centimeters indicates deposition of sediments although soil erosion patterns were not visible in this eastern part of the catchment (Fig. 9) where the surface was nearly level (almost no inclination). The deposition seems to be a result of local sediment movement as a consequence of the artificial leveling procedure, which produced irregularities at the centimeter scale. The observed crusts from the two sites generally followed the crusting pattern described previously (e.g. Bresson and Boiffin, 1990; Roth, 1997; Heil et al. 1997): The samples with higher clay and silt contents indicate a dense skin of fine material that originated from slacking through rain drops. In contrast, the samples with mainly sandy soil formed a layered depositional crust without signs of slacking.

However, for the samples from location next to lake, the physical surface crust was a combination of both the above described types (Fig. 11, 3.a-3.c); a denser structural crust underneath aeolian sediment resulting from wind erosion, which likely occurred in the catchment area (Maurer and Gerke, 2011). It accumulated

predominantly in micro-depressions. Particularly in these samples we found vesicle-shaped pores.

Vesicular pores

Vesicular pores occurred at all three sites although amounts, sizes, and distributions were different. This type of pores has often been found as a feature of desert pavements in semiarid to arid mid-latitudes (Springer, 1958; Heil et al. 1997; McFadden et al. 1998; Turk and Graham, 2011, Yonovitz and Drohan, 2009.) and arctic regions (Bockheim, 2010). The described desert soils were of fine-textured silty aeolian dust and the vesicular pores formed surface horizons of up to 20 cm thickness.

Miller (1971) explained the formation of this type of pores with air entrapment during wetting phases: A weak soil structure allows entrapped air bubbles to form spheres, the shape with the smallest surface area per unit volume. The next drying phase can stabilize the vesicles. In a rigid soil matrix entrapment of air would rather tend to fill in the preexisting pores than changing the particle arrangement. Miller (1971) also demonstrated that for a given soil the formation of vesicles enhances with increased surface tension of soil water and the number of wetting and drying cycles. The two factors - soil structure (soil particle stability) and surface tension of soil water – are the main reasons, why vesicular pore are not typical for soils in the humid region: Compared to other natural soils in the humid region, soils in the Chicken Creek catchment are mechanically instable, of single grain structure and not aggregated. The surface tension of soil solution decreases with increasing concentrations of dissolved organic matter and decreasing pH value (e.g., Anderson et al., 1995; Bachmann and van der Ploeg, 2002). The investigated soils show almost no enrichment of organic matter in the upper soil so far and pH-values of around 8, which probably lead to higher surface tensions, hence favors vesicle formation. Natural surface soils contain more or less humic substances and are depleted, such that the tension of soil water is less than that of pure water (Tschapek et al., 1978) but increased when limed (Hartge, 1958, from Bachmann and van der Ploeg, 2002).

The 2D moisture patterns observed by NR did not indicate any effect of the vesicle pores on water infiltration although vesicular horizons can reduce infiltration rates

because of air entrapment (Young et al., 2004). Probably the amounts of vesicular pores in the investigated soil samples were below a critical level to allow for air entrapment effects under the present drip irrigation rate.

Crusts effects on water infiltration and hydraulic conductivity

For the lab-scale soil slab irrigation experiment analyzed with NR, the visualized infiltration pattern show relatively homogeneous infiltration fronts in all three samples. The higher water contents in all samples next to the surface (Fig. 11) indicate increased water holding capacity of the crust. Only the flow in the sample from the lake-site seemed to be affected by the structural crust since water was ponding on the surface. The combination of the two crust types (i.e., a depositional over a structural crust) revealed a hydraulic barrier effect (i.e., water content increase above the lower permeable structural crust). Also some water droplets were observed on the soil surface probably due to local water repellency.

For the field-scale miniature infiltration experiments; however, the crust type in combination with the soil texture seems to strongly affect the surface hydraulic properties (Fig. 12). The unsaturated hydraulic conductivity values of the two sites showing a structural crust (“west” and “lake”) were significantly lower than those of the sandy site without a crust. The observation of reduced infiltration rates into crusted soil surface layers as compared to a non-crusted soil is in line with results reported elsewhere (e.g., Hoogmoed and Stroosnijder, 1984; Ben-Hur et al., 1987).

3.5. Conclusions

Soil surface structure and corresponding infiltration pattern in the artificial water catchment “chicken creek” were investigated three years after construction. Soil structure alteration in the first centimeters included development of different physical soil crusts, vesicular-shaped pores and in one case a beetle burrow. Aggregation or the development of cracks could not be observed in the soil samples studied here probably due to the predominantly sandy soil texture.

The development of a structural crust reduced the infiltration rate for unsaturated flow conditions, but did not affect the basic flow patterns as visualized in the neutron radiographic images. Infiltration patterns revealed effects of fine layered structures and of finer-textured fragments embedded in the sandy soil matrix. Here, the observed water repellency of the soil surface was spatially distributed at a local scale. The results of combined CT and NT observations suggest that the physical surface crusts in initial coarse-textured sediments modify the infiltration and moisture patterns only slightly.

We found small effects of physical soil crusts during initial stage of soil development with respect to the moisture distribution patterns in lab NR infiltration experiments but larger effects with respect to the unsaturated hydraulic conductivity by field measurements with miniature infiltrometer.

A specific feature is the occurrence of vesicular pores, which to the best of our knowledge has before only been reported for soils in arid environments. For our initial soils, the absence of organic carbon and vegetation in combination with the presence of carbonates at the soil surface seems to allow the formation of these round-shaped pores in surface layers and crusts. The results of this study may improve our understanding of initial soil structure alterations and water distributions in initial soils of developing ecosystems.

4. Effects of ground-dwelling beetle burrows on infiltration patterns and pore structure of initial soil surfaces

cf. Badorreck et al. (2012)

4.1. Introduction

Soil organisms physically change their abiotic environment by presence or activities like burrowing and mixing of materials, which in turn influences water and matter fluxes (e.g., Lee and Foster, 1991; Luo et al., 2010). Interactions between biological and physical processes are in particular affecting bare and crusted soil surfaces (e.g., Prasse et al., 2000; Langmaack et al., 2001) and most intensively probably during initial soil development stages (e.g., Fischer et al., 2010; Schaaf et al., 2011).

Interactions between soil organisms, soil and pore structures, and flow and transport properties have been emphasized in ecological science in the concept of 'physical ecosystem engineering' (Jones et al., 1994, 1997; Wright and Jones, 2006; Hastings et al., 2007). The activities of ecosystem engineers change the physical and chemical properties of soils and litter in their habitats with consequences for infiltration, water flow in soils, run off and sediment transport, hence influencing the rate of alteration and the new equilibrium state of soil processes in ecosystems (Anderson, 1988). Moreover, the soil biodiversity may have an effect on hydrological pathways, for instance, by controlling matter fluxes from terrestrial to aquatic ecosystems (Bardgett et al., 2001).

More specifically, Eldridge et al. (2010) analyzed the effect of Stipa tenacissima, biological soil crusts, and the European rabbit on the infiltration processes in grassland. Langmaack et al. (2001) reported that Collembola and Enchytraeidae contribute to rehabilitation of crusted soil surfaces and changes the soil surface micro relief. Earthworms, termites and ants are considered as the most important larger invertebrate species that are responsible for the formation of biological soil macropores (Lee and Foster, 1991); these authors concluded that burrows that penetrate soil surface crusts are particularly important for water entry to the soil. Macropores crucially affect infiltration and redistribution as these pores can provide preferential flow pathways (e.g., Beven and Germann, 1982; Flury et al.,

1994; Cey et al., 2009; Kramers et al., 2009), which can lead to local physical non-equilibrium conditions when water and solutes are by-passing most of the pore volume of the soil matrix. The mechanism of preferential flow in hydrological processes is highly complex; its initiation and extent depend not only on soil properties but also on initial and boundary conditions (c.f., Jarvis, 2007; Gerke, 2006; Köhne et al., 2009).

In temperate regions, impact of soil fauna on formation of macropores has been studied mostly with respect to earthworms. Macropore characteristics for burrows of different species were compared by means of X-ray computed tomography (e.g., Jégou et al., 1998; Capowiez et al. 2001; Bastardie et al. 2003); pore structural and biochemical modifications of the walls have been evaluated by Jégou et al. (2001) among others. Schrader et al. (2007) found a compacted zone around the caves with higher carbon and nitrogen content as well as enhanced enzymatic activities as compared with the surrounding soil matrix. This compaction could lead to reduced water movement through the walls towards the soil matrix (Bastardie et al. 2005).

The hydrological effect of earthworm burrows has frequently been reported since the early observations by Ehlers (1975). Flury et al. (1994) and Weiler and Naef (2003) conducted dye tracer experiments with different rain intensities and initial moisture conditions to observe flow in a grassland soil with mainly earthworm burrows as macropores. It was found that water entry into the macropores was initiated from the soil surface or nearly saturated soil layers and the exchange of water with the surrounding soil matrix was controlled by soil properties and soil moisture.

Knowledge about effects of soil fauna activities other than of earthworms, termites and ants on soil structure and hydrological processes are rather more limited. Brown et al. (2010) reported elevated infiltration, lower bulk density and higher soil moisture on spots where dung beetles colonized compared with beetle-free plots. Holden and Gell (2009) described similar effects of burrows from cranefly larvae, as a higher proportion of pores larger than 2 mm were found in the upper grassland soil together with higher water infiltration rates; and dye tracer experiments indicated occurrence of preferential flow along these burrows.

Little is known, however, on the macropore formation and hydraulic effects of the surface layer for initial stages of soil development (i.e., surfaces of freshly deposited sediments). In the Lusatian mining district (NE-Germany) an artificial hydrologic catchment named “Chicken Creek” was constructed to study initial ecosystem evolution and hydrological processes (Gerwin et al., 2009). Pore structural alterations of the initial soil surface are mostly unknown but assumed key processes for understanding water flow, solute transport, and vegetation establishment.

As one pioneering fauna, a ground-dwelling species classified as *Cylindera arenaria viennensis* [Schrank, 1781] was first observed in 2008 to colonize the newly developed habitat “Chicken Creek” (Elmer and Wanner, personal communication, 2009). The classification has been carried out by M. Elmer (Research Center Landscape Development and Mining Landscapes) and M. Wanner (Chair of General Ecology) from the Brandenburg University of Technology Cottbus, Germany. The ground-dwelling activity of Cicindelinae larvae results in numerous vertical pores or burrows of about one mm in diameter and several centimeters depth. For this site in the initial stage of soil and ecosystem development, both the effects of beetle burrow biopores on pore structure modifications and on water infiltration as well as the interaction between them are not well understood. In contrast to more fine-textured soils with earthworm burrows, such beetle burrows have not been analyzed intensively and occur on mostly coarse-textured and unconsolidated sandy soils or sediments only during a short development stage. One question was if the beetle larvae modify the pore structure in a way that the hydraulic properties of the surface layer are affected significantly.

Recently, non-destructive and imaging techniques are being used for the observation of pore structure and infiltration (e.g., Lehmann and Vontobel, 2000; Werth et al., 2010; Hassanein et al., 2006a). While the non-invasive X-ray micro computed tomography (CT) has frequently been utilized for quantification of macropore structures (e.g., Luo et al., 2010), neutron radiation can be used for determining the water distributions in soils. Infiltration patterns as time-series’ of two-dimensional (2D) water content distributions during the infiltration could be mapped by using neutron radiography (NR) (Lehmann et al., 2004a, 2006).

Deinert et al. (2004) determined hydraulic properties of sieved sand from analyzing 2D NR-time series' of propagating infiltration fronts. The same technique was used to visualize flow in heterogeneous lignitic mine soil samples to observe preferential flow under unsaturated steady-state conditions (Badorreck et al., 2010).

The objective of this study was to describe water infiltration and soil structure modifications in the vicinity of beetle larvae burrows and pore structure features of soil surface layers in the initial soil development stages. The moss-vegetated surface soil of young sediments with initial soil development and the infiltration patterns was analyzed for initially dry and moist conditions. Here, the effect of moss vegetation on the soil structure in the vicinity of beetle burrows was represented by samples with three degrees of moss vegetation coverage.

4.2. Materials and Methods

Site

The samples were collected in the artificially-constructed hydrologic catchment “Chicken Creek”, which is located in the Lusatian brown coal mining district about 20 km south of the city of Cottbus in Eastern Germany. The approximately 6-ha catchment area was build in 2005 and consists of coarse-textured quaternary sediments and forms a back- and foot-slope that flattens out to a pond. For detailed information on this catchment the reader is referred to Gerwin et al., 2009. The sediments of the artificial system are in the very initial stage of soil formation. The soil was classified as Entisol (US-Soil Taxonomy) or Regosol (World Reference Base for Soils, WRB, 2006). The top soil, from where the samples were taken, consists of 81% sand, 15% silt, and 4% clay (i.e., particle diameter classes are 2-0.063 mm for sand, 0.063-0.002 mm for silt, and <0.002 mm for clay; mean values of three replicates).

The catchment region where the ground-beetle burrows occur (Fig. 13a) is limited to the close vicinity of the pond due to the preference of the larvae to open littoral habitats and to soil textures between silt and fine sand (i.e., 0.2-0.02 mm particle diameter) (Müller-Kroehling et al., 2000) as well as to moisture conditions that probably provide sufficient particle stabilization.

At the time of sampling, the vegetation at the site consisted of bryophytes (i.e., moss) in a gradient from bare soil at the upper parts to densely-moss covered soil surface in lower parts next to the pond (Fig. 13b). The soil samples for neutron radiography and micro-CT analysis were collected in the vicinity of the pond in August 2008, containing at least one larvae burrow of this species (Fig. 13c).

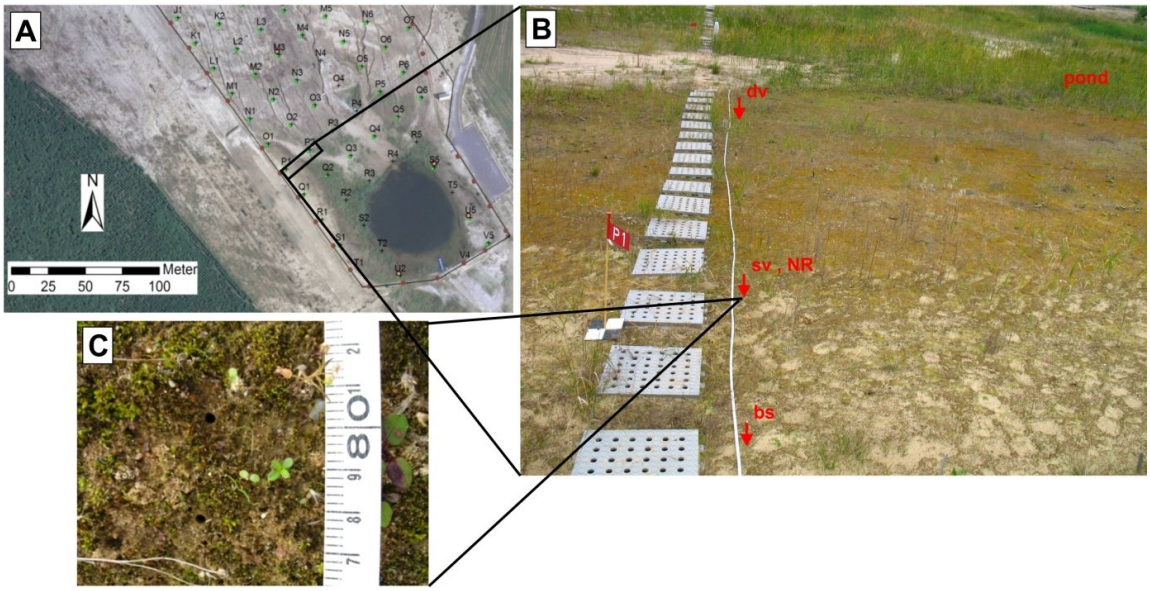

Fig. 13. Location of sampling sites within the "Chicken Creek" catchment, with (A) an aerial photo, zoomed in (B) is a detailed photo showing the three sampling points along the vegetation gradient (bs: bare soil; sv, NR: sparse vegetation, also sampling point for the neutron radiography; dv: dense vegetation), image (C) shows two larvae burrows at the soil surface.

X-ray computed tomography

The soil cores for the CT analyses were obtained at three locations from an area with bare soil (bs) and with relatively dense (dv) and sparse (sv) moss vegetation (Fig. 13) in two replicates. For sampling acrylic glass cylinder (3.5 cm in diameter and 3 cm in height) were carefully pressed into the soil surface while removing the excess soil on the sides manually with a knife. The six cores were air dried and scanned with the X-ray micro-CT-scanner (XTek HMX 225kV, now Nikon Metrology NV, Leuven, Belgium) of the Department of Soil Physics, Helmholtz Centre for Environmental Research (UFZ), Halle (Saale), Germany. The resulting 16-bit grey-scale volumes had a spatial resolution of 0.084 mm.

All CT-scans were processed successively in vertical (Z) direction as two-dimensional (2D) images (XY-planes) using plug-ins implement in the image processing package ImageJ (Version 1.4, Rasband, 1997–2009). The images were filtered to reduce the noise level with an edge-preserving anisotropic diffusion filter (Tschumperlé and Deriche, 2003). To distinguish between soil matrix and soil pore space (binarisation) the histogram-based automated thresholding method (Otsu, 1979) was applied. After segmentation, voxels were

either identified as pore (for grey values above the threshold) or as soil matrix (below threshold). The binarised images were visually inspected to assure that the pore regions were correctly identified and that the comparsison between the scans was given. To further reduce noise, we excluded isolated scattered ‘pore’ pixels with a morphological opening operation. The remaining pores had a minimum diameter of two pixels (0.168 mm). In the following we use the terms ‘macropore’ or ‘pore’ for this segmented pore space larger than 0.168 mm. The bulk density was determined by weighting the air dry sample and calculating the total volume by image analysis from the CT to account for the uneven soil surface. The volume of the moss-covered samples included also some of the above-ground biomass. Additionally the segmented pore volume was summed up for each horizontal slice to obtain porosity profiles of the samples. For a detailed investigation of the soil structure alteration due to the burrowing activity, four three-dimensional tube-shaped regions of interest (roi) in increasing distance of the cylindrical burrow (Fig. 14) were extracted from the CT volume.

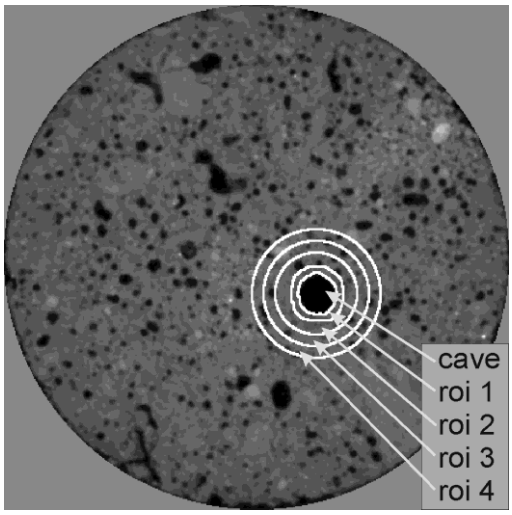

Fig. 14. Slice (xy-plane) of a Ct-scan (dark regions indicate pores in lighter soilmatrix),with burrow and four regions of interest (roi 1-4) around, indicated by red circles.

The height of the rois corresponds with the height of the scanned soil sample excluding moss cover. The roi in immediate contact with the burrow (roi_1) was derived by five morphological dilatation operations of the burrowing to preserve its slightly discontinuous shape. The other rois (roi_2 to roi_4) had straight cylindrical shape with outer diameters of 5.9, 7.5 and 9.2 mm, respectively. The center of

every roi matches the center of mass of the cavity in every XY-plane such that the slightly discontinuous shape of the burrow over the height of the sample was taken into account.

Neutron radiography

The NR-measurements were carried out at neutron radiation facility NEUTRA at the Paul Scherrer Institut (PSI, Villigen, Switzerland). Here, the radiation was generated through spallation in the neutron source SINQ where the thermal neutron beam was guided and parallelized by a collimator to the experimental station NEUTRA (Lehmann et al., 2004b). A cooled slow scan charge coupled device (CCD) camera captured the light patterns and yielded 16 bit gray-scale images with a pixel resolution of 147 µm. More detailed information of the NEUTRA facility, detector options, and applications can be found elsewhere (Lehmann et al., 2004b, 2005; Vontobel et al., 2006, 2008).

We used the NR technique to visualize water infiltration patterns in two samples that both contained a beetle burrow and that had relatively dry and moist initial conditions, respectively. The soil samples (i.e., 1 cm thick, 6 cm wide and 8 cm high) were encased by slab - type aluminum chambers with removable walls. The inner walls of the aluminum were coated with hydrophobic silicone (Dow Corning 1107 fluid, Dow Corning Corporation, Midland, USA) for eliminating capillary forces between soil and chamber wall to prevent possible bypass flow along the chamber walls under the mostly unsaturated experimental conditions.

Both undisturbed soil samples were taken at the central part of the vegetation gradient that is sparsely-covered with moss (Fig. 13). The soil was relatively coherent and allowed manual knife-cutting of rectangular intact soil blocks including the surface layer out of a vertical wall from a trench. With the front panel removed, the aluminum container was gently pressed onto the excavated squared soil volume and resized with a knife to isolate an intact soil slice that exactly fits into the chamber of 1 cm thickness. Excess soil was removed and the chamber closed with the aluminum back panel. The 6 pieces of the aluminum chamber (panels and borders of the frames) were screwed together without any further sealing to allow soil air to interact with atmospheric pressure during the infiltration experiments.

The moisture was first removed from the samples by drying the samples at 30°C for 3 days, in order to obtain a reference for the quantification of infiltration. Then, one sample was left air dry and the other was rewetted with deuterium oxide (D_2O; 99.8 vol. % D_2O, Chemotrade Leipzig Chemiehandelsgesellschaft GmbH, Leipzig, Germany) to account for a contrasting initial moisture condition. In the following we distinguish between H_2O (light water), used as tracer and D_2O (heavy water), which also 'moistened' the soil but was not quantified in our experiments. The rewetted sample was equilibrated at -30 hPa at the bottom with D_2O using a nylon membrane of 10 µm mesh size (HYDRO-BIOS Apparatebau GmbH, Kiel, Germany). The same set up was also used during the experiment as drainage. The drainage of the dry soil slab was allowed through an identical membrane which was left dry to avoid H_2O intake from the bottom.

After taking the reference images, the samples in the aluminum chamber were placed underneath a drip irrigation device consisting of 4 disposable hypodermic needles (Sterican, 0.4 mm x 20 mm, B. Braun AG, Melsungen, Germany) with a spacing of 1.2 cm each (Fig. 15) which are connected to a supply Mariotte's bottle.

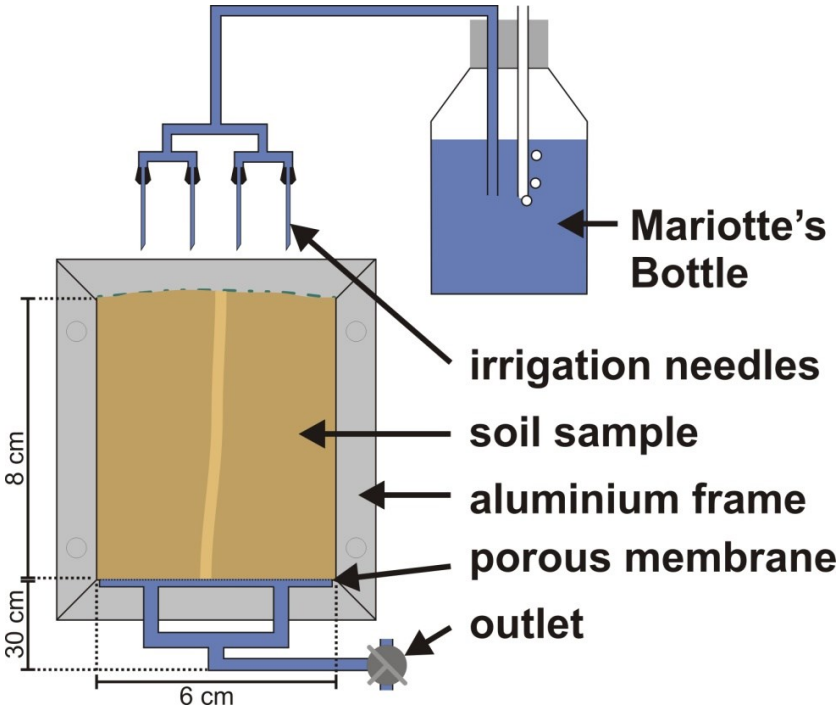

Fig. 15. Schematic drawing illustrating the experimental set-up of the neutron radiographic measurements for visualization of 2D vertical transient H_2O flow during drip-irrigation experiments.

The drip irrigation rates for the infiltration experiments were pre-selected in tests with samples of the same initial condition according to the criteria (1) to imitate realistically high rainstorm intensities while (2) preventing ponding and lateral H_2Omovement on the surface that could lead to bypass flow along chamber walls under saturated conditions. Hence, H_2O was irrigated at average rates of 14.4 mm/h for the air dry and 46.3 mm/h for the initially moist sample, which correspond to rain intensities that occur in this region once in a half-year and every ten years, respectively (Bartels et al., 1997).

Neutron-Radiographic images were taken every 13 s until the infiltration front reached the bottom of the soil slabs and changes in H_2O content distribution between two subsequent images became negligibly small. Each radiographic image from the time sequences $I(x,y,t)$ [$L^{-2}T^{-1}$] yielded a 2D distribution of the reduced neutron flux of the incident beam $I_0(x,y)$ [$L^{-2}T^{-1}$] described by Beer's law of attenuation (Lehmann et al., 2004a) as

$$I(x,y) = I_0 \cdot e^{-\Sigma(x,y)\cdot d(x,y)} \quad [7]$$

where d [L] is the thickness of the scanned material and Σ [L^{-1}] its total linear attenuation coefficient which summarizes the individual attenuation coefficients of each contained element and yields in our case for each pixel (adapted from Carminati et al., 2007):

$$-\log\left(\frac{I(x,y,t)}{I_0(x,y)}\right) = \sum_{Soil} L_{Soil}(x, y) + \sum_{Al} L_{Al}(x, y) + \sum_{H2O} L_{H2O}(x, y,t) + \sum_{D2O} L_{D2O}(x, y) \quad [8]$$

with the components *Soil*, *Al* (aluminum of the frame), H_2O (infiltrating light water), and D_2O (i.e., D_2O only in the initially wet sample). This interaction probability between the neutron radiation and the material is known for every element. The NR-images were corrected for the dark current of the CCD chip by subtraction of a dark current image, the noise was reduced with a median filter (3 x 3 pixels, 5% threshold) and a subsequent flat-field correction was applied to account for spatial heterogeneities of beam intensity and detector sensitivity. Temporal fluctuations in beam intensity were also compensated by normalization. Since the H_2O in the

sample scatters rather than attenuates the neutron radiation, a correction for sample scattering and spectral effects was performed.

We used a reference image of the initial H_2O-free condition, taken before the infiltration of H_2O. The reference image was subtracted from each of the time series' images, that the calculation of the H_2O thickness in beam direction d (Eq. [1]) and subsequent the volumetric H_2O content was possible, by taking the soil slab thickness into account. The image processing and quantification of the H_2O contents were carried out using the computer program Quantitative Neutron Imaging (QNI, Version 1.0) (Hassanein et al. 2005; Hassanein, 2006b). D_2O which was displaced by H_2O during the infiltration experiment, and maybe caused a slight bias, was not taken into account. Moreover, water repellency of the dry soil sample was tested by using the water drop penetration time (WDPT) test (Dekker and Ritsema, 1994) performed directly after the neutron radiography experiment. Therefore one large side of the container was opened and droplets were randomly placed on regions which were left dry, hence excluded from infiltrating water.

4.3. Results

Soil structure

The bulk density (measured air dry) varied between 1.45 – 1.48 g cm^{-3} for dense and sparse moss vegetation and 1.2 g cm^{-3} for bare soil samples (i.e., dv1: 1.44 g cm^{-3}, dv2: 1.47 g cm^{-3}, sv1: 1.46 g cm^{-3}, sv2: 1.5 g cm^{-3}, bs1: 1.09 g cm^{-3}, and bs2: 1.31 g cm^{-3}). The macro pore volumes (Fig. 4) derived from the CT-evaluation of the vertical profiles reflect the lower bulk density of the samples from the non-vegetated patch.

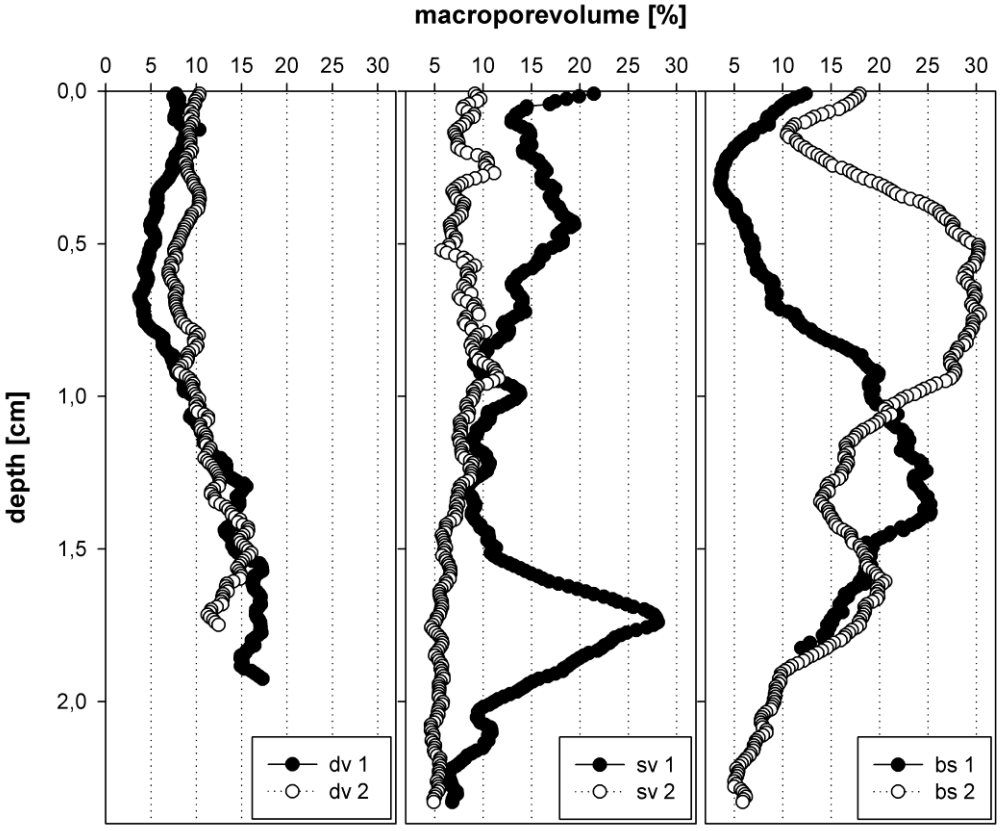

Fig. 16. Vertical depth profiles of macropore volume including beetle burrow of the samples with dense vegetation (dv), sparse vegetation (sv) and bare soil (bs) in two replicates.

The internal structure visualized by cross sections of the micro-CT scans revealed the following characteristic structures for the three sampling sites. The selected cross sections (Fig. 17) illustrate the soil structure excluding the central beetle burrow (with the exception dv1).

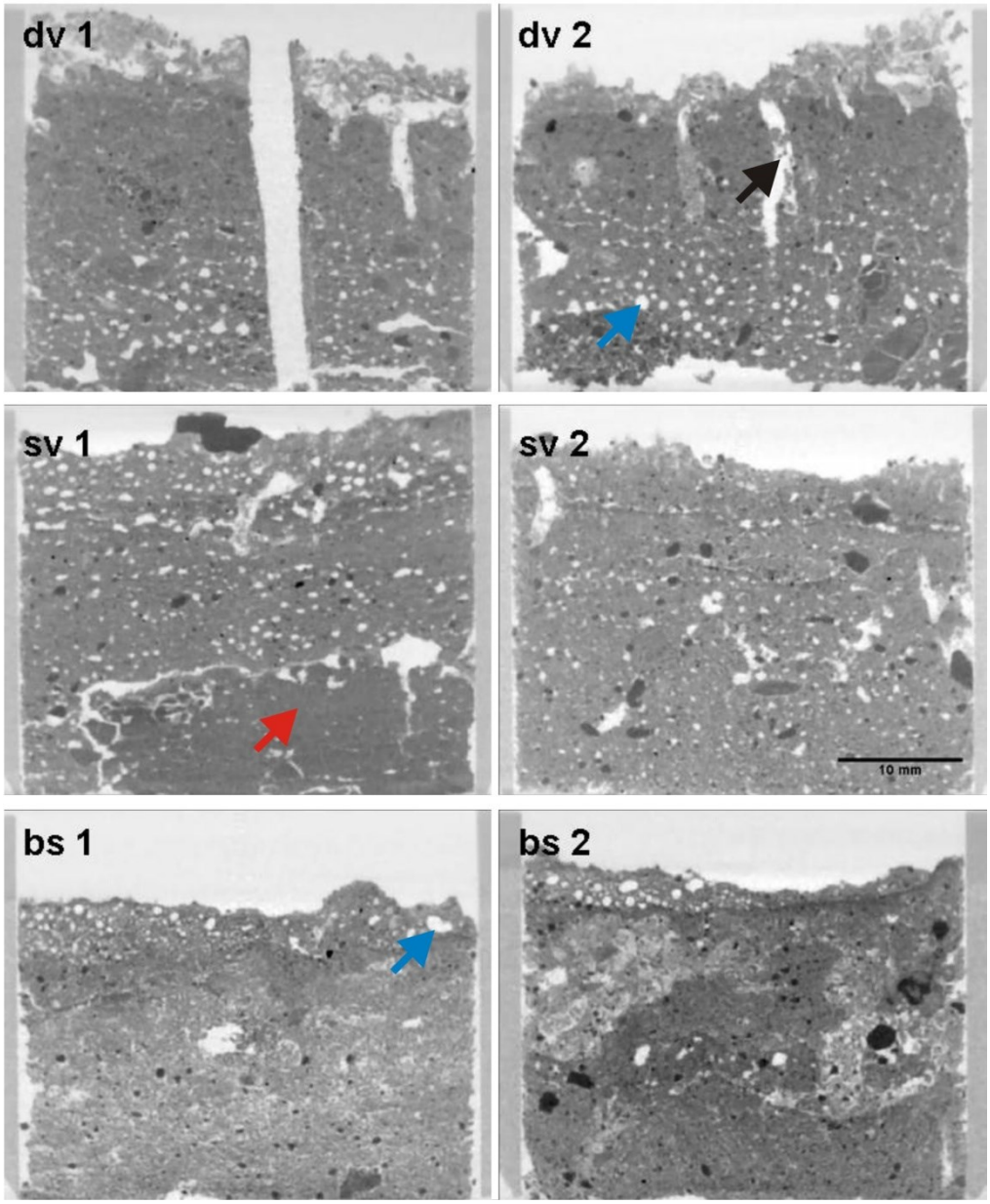

Fig. 17. CT-cross-sections of the samples with dense moss-vegetation (dv1, dv2), sparse vegetation (sv1, sv2) and bare soil (bs1, bs2); black arrow indicates a decayed burrow, red arrow a clay clod and the blue arrows point at vesicular pores.

Both samples with dense vegetation cover (dv1, dv2) show the moss on top in a layer with high porosity and in case of dv1 in form of horizontal voids between a more organic and a more mineral soil matrix. The mineral soil underneath the moss root zone seems to have a lower porosity in the first centimeter except for some regions of smaller vertically elongated caves. The density distribution changes towards the bottom part of both cores such that the pore structure

includes numerous isolated, evenly distributed vesicular pores. The macro pore volumes delineated in the depth profiles (Fig.16), are slightly reduced in the uppermost centimeter (3-10 vol%) of the mineral soil compared to the bottom part with 10-20%. The values in Figure 16 quantitatively describe the general visual impression gained from the cross sections (Fig. 17).

A clear stratification is absent in the two samples with sparse vegetation (Fig.17, sv1 and sv2). Here, the main fraction of macropore space consists of unconnected vesicular pores which were evenly distributed. Few of the macro pores were found to be also burrow-like vertically elongated, but were less numbered than in the moss covered samples. A special feature of sv1 is a clay clod, which fills most of the volume of the bottom part. The pore volume profiles of the two sparsely vegetated soil samples (Fig. 16), differed distinctly from each other such that for sv2 the pore volume decreased more or less linearly from around 10 to 5 vol.%. The vertical profile of sample sv2 (Fig. 17), reflects a heterogeneous structure with pore volumes up to 28% in 1.8 cm depth due to the relatively large pore space on top of the clay clod.

The soil structure in the non-vegetated part of the transect (Fig. 13) was extremely heterogeneous (Fig. 17, bs1 and bs2), showing regions with an extensive pore network next to denser regions overlain by a denser layer and covered by an erosion sediment with vesicular pores. In both samples of the bare soil, the pore volume decreases with depth in the first millimeters and rises then again peaking, however, at different depths (Fig. 16).

The CT-scans revealed also morphological and structural modifications of the burrowing activity in the uppermost soil. To visualize the influence of the beetle burrows on the surrounding soil structure we computed the pore volume of four cylindrical ROIs in increasing distance to the burrow (Fig. 18).

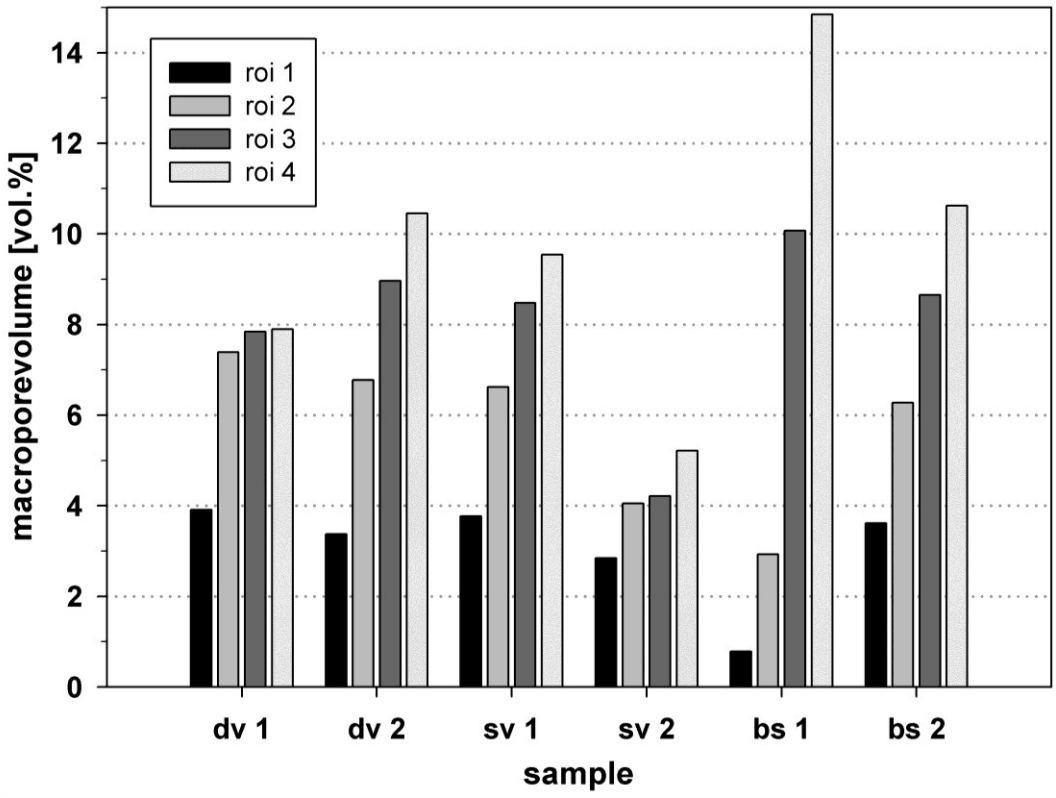

Fig. 18. Macropore volume of regions around the beetle burrows of CT-scanned samples (dv 1,2: dense vegetation cover; sv 1,2: sparse vegetation cover; bs 1,2 bare soil); regions of interest (roi) next to the burrow (roi 1) to 9.2 mm away (roi 4).

The pore volume of roi_4 in 9.2 mm distance was considered as the pore volume of the bulk soil, hence not influenced by the burrowing activity. The burrows with an average diameter of one mm were relatively vertical. In all cases, the walls of the relatively 'fresh' beetle burrows exhibited the lowest macro porosity; the volume of macropores increased with distance from the biopore, although with different magnitudes. The beetle burrow influenced the surrounding pore system in the more compacted soil of sample sv2 to a lesser degree than in sv1, which was comparable with the samples of the dense vegetated area (dv). The degrees of compaction locally in the vicinity of the burrow (i.e., here determined as the decrease in the macropore volume between roi's 4 and 1) were found to be largest in the samples without vegetation (bs1 and bs2) (Fig. 18).

Infiltration patterns

Soil slab images (Figs. 19 and 20) show proceeding H_2Oinfiltration fronts during the first 32 min of the experiment. In both samples flow seemed to be affected by the channel, however, in a specific way.

For the initially D_2O moist sample (Fig. 7), the burrow's position was not exactly straight vertical relative to the container: The burrow hit the wall of the container approximately in the middle of the sample, also visible in the H_2O-free radiograph (Fig. 7, upper left), where the lighter shaded burrow disappeared half-way towards the bottom.

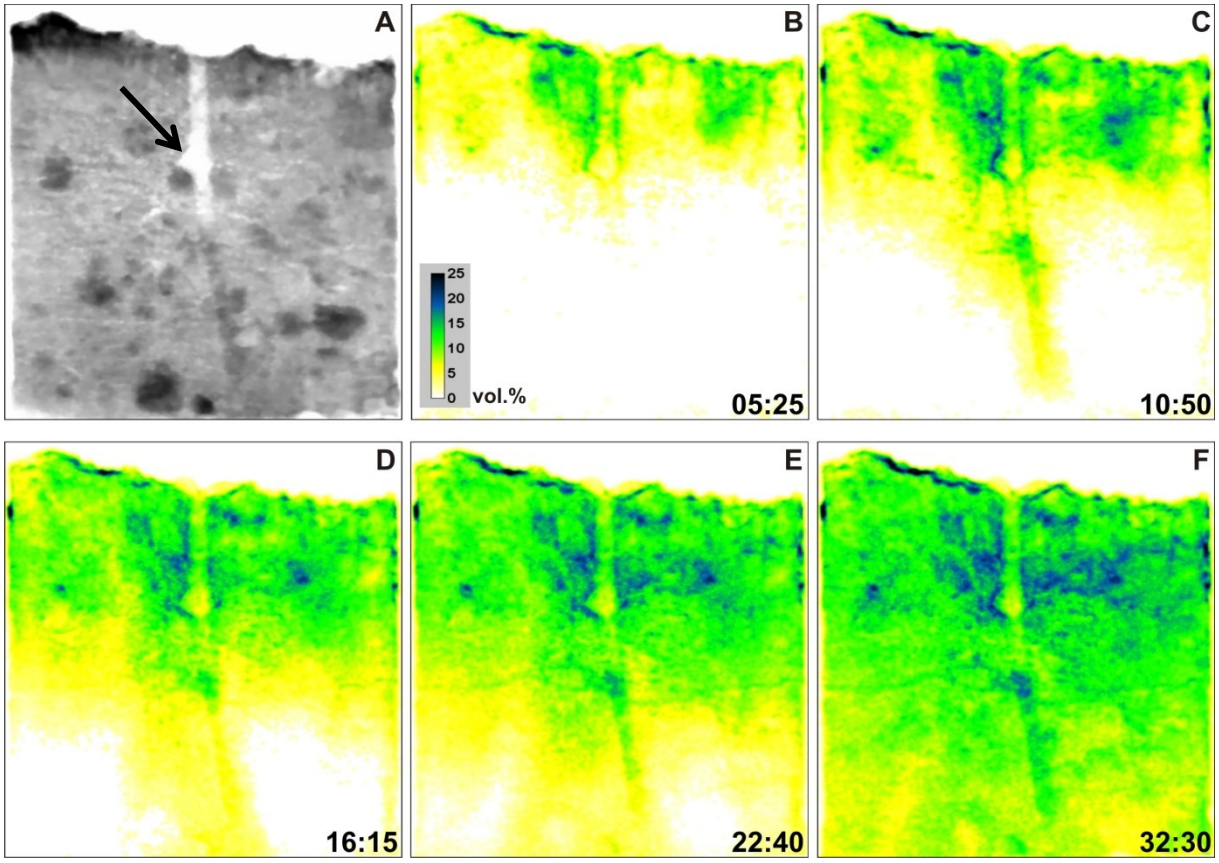

Fig. 19. Reference H_2O-free radiography (A; left, top) and time series (B-F) of the initially D_2O moist sample with 2D volumetric H_2O content distributions at time steps (mm:ss); black arrow indicates channel

The H_2O infiltration front resulting from an irrigation rate of 46.3 $mm*h^{-1}$ appeared to be relatively homogeneous although a slight accumulation of irrigated soil moisture in the first mm of the soil was visible especially on the surface on the left-hand side (Fig. 19, C). The burrow initially remained relatively dry in the first cm of the sample. However, the H_2O front propagated more rapidly in the vicinity of the

channel and reached the bottom of the container 12 minutes after start of the experiment. Only in the midterm of the experiment, the burrow acted as a preferential flow pathway (Fig. 19, C and D). In the bottom part of the container, higher H_2O contents in the narrow part of the burrow than in the surrounding soil matrix were indicating increased H_2O saturation in the burrow.

For the initially dry soil sample (Fig. 20, A), the burrow's position was relatively straight vertical and ended in a disturbed zone at the bottom of the container.

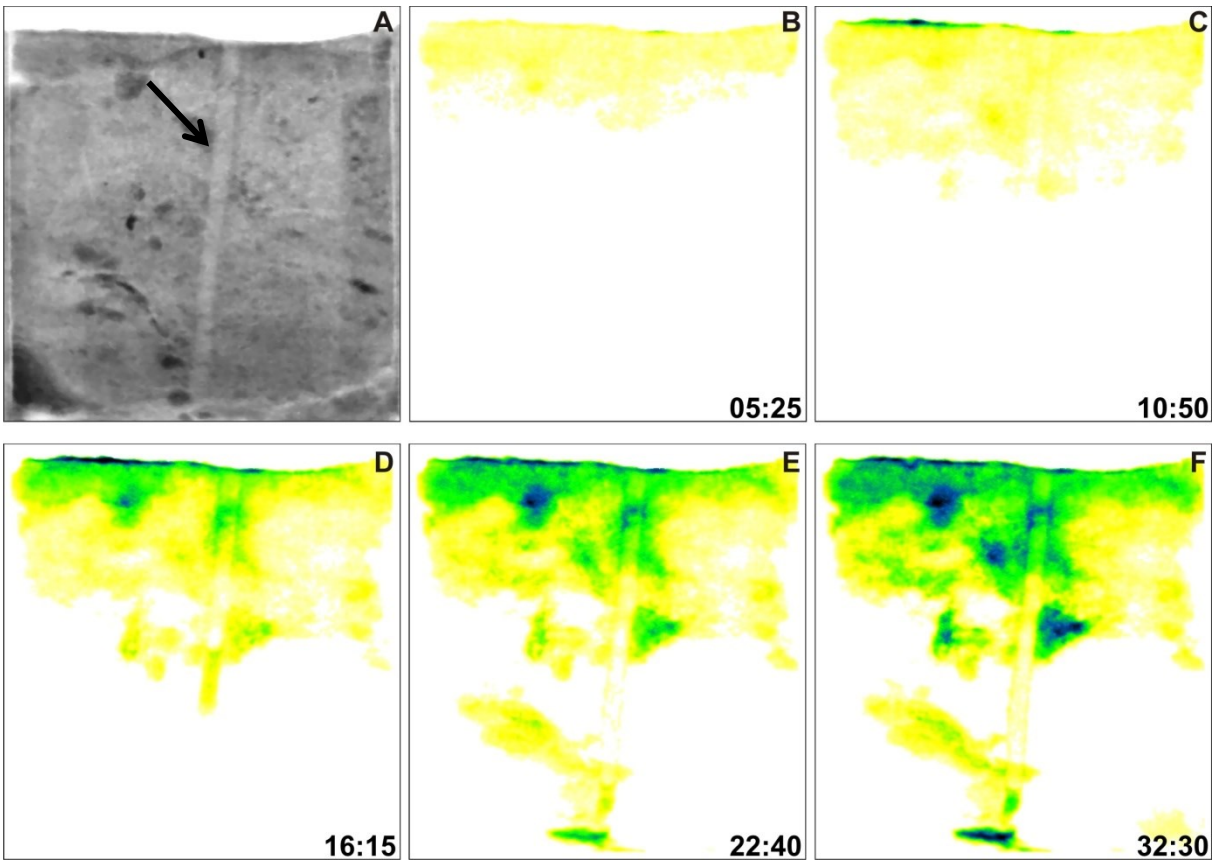

Fig. 20. Reference H_2O-free radiography (A; left, top) and time series (B-F) of the initially dry sample with 2D volumetric H_2O content distributions at time steps (mm:ss); black arrow indicates channel.

The infiltration front here resulted from a lower irrigation intensity (14.4 $mm*h^{-1}$) that was required to avoid surface H_2O ponding. Nevertheless, a thin layer with higher water contents at the soil surface was visible (Fig. 20, B). The water infiltration in the dry slab was then far more heterogeneous than the one in the D_2O moist slab. Locally, H_2O water accumulations with volumetric water contents

up to 25% were observed. At the start of the experiment, the burrow remained completely H_2O -free; this situation lasted until local water accumulation at the right hand side of the burrow reached saturation and water started to enter the burrow and to move rapidly downwards towards the bottom. An interesting observation was the rapid H_2O absorption by a defined region in the surrounding soil matrix during the passage of the first water front in the burrow. For those regions that remained dry during the NR experiment, the results of the WDPT test revealed strong water repellency (i.e., droplets stayed for at least 15 min).

4.4. Discussion

The results of this study illustrate the role of initial soil surface structures on the soil micro morphology and water infiltration pattern under variable initial moisture conditions. The interaction between pore structures and hydrological processes is of particular interest for hydrological catchments with rapidly developing soil surfaces structures. The initial feedback reactions are based on small-scale interactions between abiotic and biotic processes and components. Their effects on larger-scale fluxes and ecosystem development were studied in an interdisciplinary collaborative approach using an artificially-created experimental hydrological catchment (Fischer et al., 2010; Gerwin et al., 2009; Schaaf et al., 2011).

Soil structure

The soil macropore structure showed pronounced heterogeneity, which is characteristic for overburden sediment. Particularly the surface layers of these sediments are subject to leveling and mixing of the construction activities. Moreover environmental forces like erosion, plant roots, soil fauna, shrinking and swelling amplify the heterogeneous soil pore system and promote structural development of young sediments in this initial phase. Both, man-made and some natural induced structures were found in the samples of the micro-CT analysis (Fig. 17).

The clay clod that is particularly observable in one sample with sparse vegetation (sv1) is a result of the construction of the catchment. Clay fragments of various shapes and sizes originate from the mixing of overburden sediments during the dumping procedure, and are a characteristic feature of the soils in the Chicken Creek catchment (e.g., Schaaf et al., 2011). The fragments represent a massive barrier for water flow, but could also trigger preferential flow, due to cracks in the vicinity, and between fragment and surrounding soil matrix (Badorreck et al. 2010; Guebert and Gardner, 2001). This macro pore system could also be detected in the sv1 sample around the clay clod. Moreover local mixing of different sediments could be visualized in sample bs2.

Other pore structural features can be explained as a result of pore modifications due to the influence of bryophytes and beetle caves. Erosion patterns were

observed only in the samples with the bare soil visible as a depositional layer on the surface (Fig. 17). The bryophyte cover even if sparse seems to protect the soil surface and prevent sediment movement. A denser moss cover compacts the first centimeter of the soil with their roots. Compaction of the soil by the moss probably led to a retarded degradation of burrows (i.e., disaggregation processes are slower as compared to those in samples without moss vegetation) such that burrows in various decaying stages could be observed in the samples (Fig. 17).

A quite common feature of this soil seemed to be round shaped so-called vesicular pores. Such isolated macro pores were found in the bottom part of the moss-covered sample and more evenly distributed in the sparsely vegetated sample and in a depositional layer on top of bare soil. The existence of vesicular pores could reflect a weaker/loose soil structure. The development of vesicular pores has been described for crusts of desert soils where they develop when air bubbles are trapped within wetted plasmic soil and can take a shape with minimum potential energy (Valentin, 1991). This is possible in a soil matrix where the particles can be pushed aside to form bubbles during rain events and can be stabilized upon drying. Such a mechanism could have been likely to occur at the study site as well because of both soil and climatic conditions, at least temporarily during bare soil and dry summer.

The burrowing activity of *Cylindera arenaria viennensis* leads mostly to vertical channels with locally compacted walls, which was more pronounced in bare soil (Fig. 18, right hand side). It is likely that the particles in this weaker soil structure were rather be pushed aside than conveyed out of the burrow.

Infiltration patterns

Neutron radiography showed preferential flow in the initially moist and dry soil sample. However, for the interpretation of the results one have to consider possible effects of the experimental set up: (i) Firstly we used a more than three times higher precipitation rate for the D_2O moist soil sample than for the dry one, which probably lead to different flow pattern. The higher H_2O infiltration rate could more likely initiate preferential flow, than it would with the same rate used for the dry sample. (ii) Moreover the bottom boundary condition for the dry soil was differed such that we used -30 hPa for the D_2O moist soil sample and free

drainage for the dry soil. This likely caused a slight ponding effect at the bottom of the dry soil at the end of the experiment. (iii) We neglected the displacement of heavy water of by H_2O in the D_2O wetted soil. This artifact is discussed in Badorreck et al. (2010) in more detail. Nevertheless, despite the described restrictions the results allowed some interesting outcomes.

Both samples were collected in the middle of the transect, hence they were sparsely covered with moss. Taking the results of the micro-CT measurements into account, it is likely, that the burrow walls were also compacted and evenly distributed vesicular pores could be found in the soil slabs for the neutron radiography (Figs. 19 and 20).

In the moist soil sample, the slightly non-vertical burrow seems to first narrow and finally end in the side wall of the container in the middle of the sample. This might promote a local ponding in the burrow at the end of the experiment. The flow in the compacted zone along the burrow could under certain conditions become accelerated as compared to the matrix if the unsaturated conductivity of the compacted soil material is higher. In contrast, the isolated vesicular macropores in the surrounding soil tend to lower the hydraulic conductivity under the applied irrigation intensity because they remain mostly air-filled (Fig. 17). With increasingly higher water saturation, the effect of the pore structure on the hydraulic properties might turn vice versa, because of an increasingly continuous water-filled macroporosity. Similarly for earthworm burrows, Bastardie et al. (2005) explained the observed reduced water movement through burrow walls at higher water saturations by the effect of compacted soil in the vicinity of the burrow wall.

The initially dry soil (Fig. 20) showed different infiltration patterns with time: The mostly dry and water repellent subsoil functioned as internal barrier and led to an accumulation of infiltrating water in the upper part of the topsoil; Accumulation continued until a threshold water content of approximately 25 vol.% was exceeded and water started entering the burrow by gravity.

The water drop penetration time tests revealed severe water repellency in the bottom part of the sample; this local water repellency may probably explain the observed bypass flow. The fact that water repellency was observed only in the air-dried sample is indicative for effects of organic matter as the reason. Although,

organic C was below detection limits and the C contents of the initial soil in general was relatively low (Gerwin et al., 2011), small amounts of organic matter as coatings on soil particles can affect wettability of soil regions; the strong small-scale spatial heterogeneity of the water repellency has been reported for similarly deposited overburden sediments before (e.g., Hangen et al., 2004; Gerke et al., 2001). The isolated region left-hand-side next to the burrow that was rapidly wetted during passage of burrow water (Fig. 20, E) was probably a wettable region located inside an otherwise water repellent matrix. This could be a result from mixing of different parent materials during sediment dumping. The initial 'snap-off' effect reflects non-uniform gravity-driven flow as previously reported by Weiler and Neaf (2003) for natural soils among others. The observed preferential flow along the beetle burrow demonstrates the strong influence of the soil biota in forming hydrological pathways, which is in line with results of previous investigations of Bardgett et al. (2001). The effects of Cylindelidae larvae activity on soil hydraulic properties are comparable with respect to increasing water infiltration to that of other beetles (e.g., Brown et al. 2010). Of particular importance is the effect of 'ecological engineers' as macropore-forming and moreover interacting factor for water infiltration in modifying biological soil crusts (e.g., Eldridge et al., 2010; Fischer et al., 2010) and modifying the soil surface by providing pore structures for infiltration pathways to increase deeper soil accessibility for next stages of soil development.

4.5. Conclusions

We studied water infiltration and soil structure modifications in the vicinity of beetle larvae burrows as well as pore structure features of soil surface layers in the initial soil development stages.

The results suggest that the bryophyte cover even if sparse protects the soil surface and prevents sediment movement. With a dense moss cover the first centimeter of the soil appeared denser. Here, larger pores even if in a decayed state have been conserved in the surface layer. The CT-images suggest the existence of cracks around finer-textured fragments and vesicular pores as isolated or horizontally-layered macropores that otherwise are known from arid areas as indicator for heterogeneous (fragments) and mechanically instable (vesicles) soil structure. The burrowing activity of *Cylindera arenaria viennensis* leads to locally compacted walls, where the surrounding soil was less stable as in the bare soil as compared to the moss covered soil. The burrowing activity seems to depend characteristically on local conditions; a weaker structure allows the larvae to push soil particles aside rather to actively remove particles by conveying them out of the burrow. The initial soil structural development (i.e., biopores and moss cover) resulting from activities of these ‘ecological engineers’ considerably affects water infiltration and modifies the patterns of water movement in the soil. The observed preferential flow along burrows demonstrate the effect of soil water repellency and structural influences of soil forming fauna and flora, which open dynamic pathways for successively deeper soil development.

5. Concluding remarks

Since specific conclusions of the three studies have already been given in the respective chapters, the following remarks present a brief summary of the results and an overall synopsis.

One aim of the dissertation was to visualize the soil structure and flow patterns in soils with differently formed pore networks:

I. A mine soil with cracked lignitic fragments embedded in a compacted sand-dust matrix was analyzed resulting in the observation of flow paths of different nature. Finger-like flow paths developed in the sandy matrix and flow patterns which exclude the lignitc fragments were illustrated, under steady state flow conditions. The 3D neutron radiography of a multistep experiment revealed preferential flow paths in the vicinity of a lignitc fragment and supports the results the flow setup with -30 hPa. Both investigations indicated that a second more continuous pore network persisting between dried fragments and bulk matrix for the BBt mine soil might exist.

II. Another study investigated influences of soil surface structures on infiltration patterns in the artificial water catchment “chicken creek” three years after site construction. Soil structure alteration in the first centimeters included development of different physical soil crusts, vesicular-shaped pores and in one case a beetle burrow. Since hydrological processes at the soil surface take place under rather unsteady flow conditions, we conducted infiltration experiments using drip irrigation. The results of combined CT and NT observations suggest that physical surface crusts in initial coarse-textured sediments modify the infiltration and moisture patterns in the NR experiments only slightly but reduced the unsaturated hydraulic conductivity in field measurements with a miniature infiltrometer. A specific feature found in the soil samples were vesicular pores. So far this finding has only been reported for soils in arid environments.

III. In a last study we investigated the water infiltration and soil structure modifications in the vicinity of *Cylindera arenaria viennensis* beetle larvae burrows as well as pore structure features of soil surface layers in the same artificial water catchment “chicken creek”. The CT-images revealed even more vesicular pores than in the soil crusts of the second study as isolated or horizontally-layered

macropores. They are known as indicator of a mechanically instable soil structure. The burrowing activity of *Cylindera arenaria viennensis* leads to locally compacted walls, where the surrounding soil was less stable as in the bare soil as compared to the moss covered soil. The neutron radiographs of infiltration time series visualized pronounced preferential flow around the burrow only in the initially dry soil.

The presented experiments on flow patterns in differently structured mine soils reflect the inherent heterogeneity in soils of artificial origin. The two soils mainly structured by abiotic soil forming factors - parent material (with lignitc fragments) in the first, and soil crusting investigated in the second study – exhibit preferential flow, however to a different degree. Even in these "young" soils effects of shrinking and welling or soil erosion influenced water flow pattern. The additional effects of "ecological engineers" such as *Cylindera arenaria viennensis* and moss vegetation on the structure of only a few years old mine soil lead to inherent preferential flow processes. The combination of visualization techniques quantifying the structure and the flow patterns played the key role for understanding the observed processes.

Another strong focus of the dissertation was set on the development of methods for using neutron radiography and neutron tomography for undisturbed soil samples exhibiting heterogeneities. For the first time neutron radiography was applied to undisturbed natural soil samples. Therefore some experimental equipment had to be constructed and tested. Also new measurement protocols had to be designed. In addition the overall strengths and limitations of such a method had to be evaluated.

The construction of a suitable aluminum container found to be crucial for all 2D and 3D experiments using neutron radiation. Here, the ideal thickness of the sample in beam direction limited the quantification of water. The observed detector saturation occurred while measuring water flow in the mine soils with lignitic fragments, due to strong background attenuation of contained organic carbon. A reduced sample thickness and infiltration with deuterium diluted H_2O seem to be a solution. The limit towards thinner samples is determined by the soil sampling procedure. The preparation of an undisturbed soil sample was found to be

possible to a thickness of 1 cm in the relatively homogenous soil with the beetle burrows. Otherwise, the major progress of the NT technique in relation to dye tracer experiments is the opportunity to trace water itself, instead of a chemical compound susceptible to chemical retardation.

In conclusion, the combination of soil structural information from CT measurements with flow patterns from NT time series proved to be a suitable way to quantify preferential flow in heterogeneous porous media and to understand the underlying structure leading to the observed processes.

6. References

Aldous, P.J., and P.L. Smart. 1988. Tracing ground-water movement in abandoned coal mined aquifers using fluorescent dyes. Ground Water 26:172-178.

Anderson, M.A., Hung, A.Y.C., Mills, D., and M.S. Scott. 1995. Factors affecting the surface tension of soil solutions and solutions of humic acids. Soil Sc. 160: 111-116.

Androutsopoulos, G.P., and T.J. Linardos. 1986. Effects on drying upon lignite macro-pore structure. Powder Technol. 47:9-15.

Ankeny, M.D., M. Ahmed, Kaspar, T.C., and R. Horton. 1991. Simple field method for determining unsaturated hydraulic conductivity. Soil Sci. Soc. Am. J. 55: 467-470.

Assouline, S., and Y. Mualem. 2000. Modeling the dynamics of soil seal formation: analysis of the effect of soil and rainfall properties. Water Resour. Res. 36: 2341-2349.

Assouline, S., and Y. Mualem. 2002. Infiltration during soil sealing: the effect of areal heterogeneity of soil hydraulic properties. Water Resour. Res. 38: 1286, doi:10.1029/2001WR001168.

Assouline, S. 2004. Rainfall-induced soil surface sealing: a critical review of observations, conceptual models, and solutions. Vadose Zone J. 3: 570-591.

Augeard, B., Assouline, S., Fonty, A., Kao, C., and M. Vauclin. 2007. Estimating hydraulic properties of rainfall-induced soil surface seals from infiltration experiments and x-ray bulk density measurements. J. Hydrol. 341: 12-26.

Badorreck, A., Gerke, H.H., and P. Vontobel. 2010. Noninvasive observations of flow patterns in locally heterogeneous mine soils using neutron radiation. Vadose Zone J. 9: 362-372, doi:10.2136/vzj2009.0100.

Badorreck, A., Gerke, H.H., and R.F. Hüttl. 2012. Effects of ground-dwelling beetle burrows on infiltration patterns and pore structure of initial soil surfaces. Vadose Zone Journal 11, doi: 10.2136/vzj2011.0109.

Badorreck, A., Gerke, H.H., and R.F. Hüttl. 2013. Morphology of physical soil crusts and infiltration patterns in an artificial Catchment. Soil & Tillage Research 129: 1-8.

Bachmann, J., and R.R. van der Ploeg. 2002. A review on recent developments in soil water retention theory: interfacial tension and temperature effects. J. Plant Nutr. Soil Sci. 165: 468-478.

Bardgett, R.D., Anderson, J.M., Behan-Pelletier, V., Brussaard, L., Coleman, D.C., Ettema, C., Moldenke, A., Schimel, J.P., and D.H. Wall. 2001. The influence of soil biodiversity on hydrological pathways and the transfer of materials between terrestrial and aquatic ecosystems. Ecosystems 4: 421-429.

Bartels, H., Malitz, G., Asmus, S., Albrecht, F.M., Dietzer, B., Günther, T., and H. Ertel. 1997. Koordinerte Starkniederschlags-Regionalisierungs-Auswertungen (KOSTRA). Selbstverlag des Deutschen Wetterdienstes, Offenbach am Main, Germany. (in German)

Bastardie, F., Capowiez, Y., de Dreuzy, J.-R., and D. Cluzeau. 2003. X-ray tomographic and hydraulic characterization of burrowing by three earthworm species in repacked soil cores. Appl. Soil Ecol. 24: 3-16.

Bastardie, F., Ruy, S., and D. Cluzeau. 2005. Assessment of earthworm contribution to soil hydrology: a laboratory method to measure water diffusion through burrow walls. Biol. Fertil. Soils 41: 124-128.

Bear, J. 1972. Dynamics of fluids in porous media. Dover Publ. Inc., New York.

Beven, K., and P. Germann. 1982. Macropores and water flow in soils. Water Resour. Res. 18: 1311-1325.

Blodau, C. 2006. A review of acidity generation and consumption in acidic coal mine lakes and their watersheds. Sci. Total Environ. 369: 307-332.

Bockheim, J.G. 2010. Evolution of desert pavements and the vesicular layer in soils of the Transarctic Mountains. Geomorphology 118: 433-443.

Bresson, L.-M., and J. Boiffin. 1990. Morphological characterization of soil crust development stages on an experimental field. Geoderma 47: 301-325.

Bresson, L.M., and L. Cadot. 1992. Illuviation and structural crust formation on loamy temperate soils. Soil Sci. Soc. Am. J. 56: 1565-1570.

Brown, J., Scholtz, C.H., Janeau, J.-L., Grellier, S., and P. Podwojewski. 2010. Dung beetles (Coleoptera: Scarabaeitdae) can improve soil hydrological properties. Appl. Soil Ecol. 46: 9-16, doi: 10.1016/j.apsoil.2010.05.010.

Buczko, U., Gerke, H.H., and R.F. Hüttl. 2001. Spatial distributions of lignite mine spoil properties for simulating 2-D variably saturated flow and transport. Ecol. Eng. 17: 103-114.

Buczko, U., and H.H. Gerke. 2005. Estimating spatial distributions of hydraulic parameters for a two-scale structured heterogeneous lignitic mine soil. J. Hydrol. 312: 109-124.

Buczko, U., and H.H. Gerke. 2006. Modelling two-dimensional flow and bromide transport in a heterogeneous lignitic mine soil. Vadose Zone J. 5: 14-26.

Capowiez, Y., Monestiez, P., and L. Belzunces. 2001. Burrow systems made by Aporrectodea nocturna and Allolobophora chlorotica in artificial cores: morphological differences and effects of interspecific interactions. Appl. Soil Biol. 16: 109-120.

Carminati, A., Kaestner, A., Hassanein, R., Ippisch, O., Vontobel, P., and H. Flühler. 2007. Infiltration through series of soil aggregates: Neutron radiography and modeling. Adv. Wat. Res. 30: 1168–1178.

Cey, E.E., and D.L. Rudolph. 2009. Field study of macropore flow processes using tension infiltration of a dye tracer in partially saturated soils. Hydrol. Process. 23: 1768-1779.

Chen, Y., Tachitzki, J., Brouwer, J., Morin, J., and A. Banin. 1980. Scanning electron microscope observations on soil crusts and their formation. Soil Sci. 130: 49-55.

Cnudde, V., Dierick, M., Vlasenbroeck, J., Masschaele, B., Lehmann, E., Jacobs, P., and L. Van Hoorebeke. 2008. High-speed neutron radiography for monitoring the water absorption by capillarity in porous materials. Nucl. Instrum. Methods Phys. Res.Sect. B 266: 155-163.

Conesa, H.M., Moradi, A.B., Robinson, B.H., G. Kühne, Lehmann, E., and R. Schulin. 2009. Response of native grasses and Cicer arietinum to soil polluted with mining wastes: Implications for the management of land adjacent to mine sites. Environ. Exp. Bot. 65: 198-204.

Deinert, M.R., Parlange, J.-Y., Steenhuis, T.S., Throop, J., Unlu, K., and K.B. Cady. 2004. Measurement of fluid contents and wetting front profiles by real-time neutron radiography. J. Hydol. 290: 192-201.

Dekker L.W., and C.J. Ritsema. 1994. How water moves in a water repellent sandy soil: 1. Potential and actual water repellency. Water Resources Research 30: 2507–2517.

Dowd, B.A., Campbell, G.H., Marr, R.B., Nagarkar, V., Tipnis, S., Axe, L., and D.P. Siddons. 1999. Developments in synchrotron x-ray computed microtomography at the National Synchrotron Light Source. Proceedings of the SPIE Conference on Developments in X-Ray Tomography II. 3772: 224-236.

Ehlers, W. 1975. Observations on earthworm channels and infiltration on tilled and untilled Loess soil. Soil Sci. 119: 242-249.

Eldridge, D.J., Bowker, M.A., Maestre, F.T., Alonso, P., Mau, R.L., Papadopoulos, J., and A. Escudero. 2010. Interactive effects of three ecosystem engineers on infiltration in a semi-arid mediterranean grassland. Ecosystems 13: 499-510.

Evangelou, V.P. 1995. Pyrite oxidation and its control. CRC Press, Boca Raton, FL.

Fischer, T., Veste, M., Schaaf, W., Dümig, A., Kögel-Knabner, I., Wiehe, W., Bens, O., and R.-F. Hüttl. 2010. Initial pedogenesis in a topsoil crust 3 years after construction of an artificial catchment in Brandenburg, NE Germany. Biogeochemistry 101: 165-176, DOI: 10.1007/s10533-010-9464.

Flury, M., Flühler, H., Jury, W.A., and J. Leuenberger. 1994. Susceptibility of soils to preferential flow of water: A field study. Water Resour. Res. 30: 1945-1954.

Gerke, H.H., Molson, J.W., and E.O. Frind. 1998. Modeling the effect of chemical heterogeneity and acidification and solute leaching in overburden mine spoils. J. Hydrol. 209: 166-185.

Gerke, H.H., Molson, J.W., and E.O. Frind. 2001. Modeling the impact of physical and chemical heterogeneity on solute leaching in pyritic overburden mine spoils. Ecol. Eng. 17: 91-101.

Gerke, H.H., Hangen, E., Schaaf, W., and R.F. Hüttl. 2001a. Spatial variability of potential water repellency in a lignitic mine spoil afforested with Pinus nigra. Geoderma 102: 255-274.

Gerke, H.H. 2006. Preferential flow descriptions for structured soils. J. Plant Nutrition Soil Sci. 169: 382-400.

Gerke, H.H. 2006a. Exploring Preferential flow in forest-reclaimed lignitic mine soil. Adv. Geoecol. 38: 380-387.

Gerke, H.H., Badorreck, A., and M. Einecke. 2009. Single- and dual-porosity modeling of flow in reclaimed mine soil cores with embedded lignitic fragments. J. Cont. Hydrol. 104: 90-106.

Gerwin, W., Schaaf, W., Biemelt, D., Fischer, A., Winter, S., and R.F. Hüttl. 2009. The artificial catchment „Chicken Creek“ (Lusatia, Germany) – A landscape laboratory for interdisciplinary studies of initial ecosystem development. Ecol. Eng. 35: 1786-1796.

Gerwin, W., Schaaf, W., Biemelt, D., Winter, S., Fischer, A., Veste, M., and R.F. Hüttl. 2011. Overview and first results of ecological monitoring at the artificial watershed Chicken Creek (Germany). Phys. Chem. Earth 36: 74-86.

Guebert, M.D., and T.W. Gardner. 2001. Macropore flow on a reclaimed surface mine: infiltration and hillslope hydrology. Geomorphology 39: 151-169.

Hallett, P.D., Nunan, N., Douglas, J.T., and I.M. Young. 2004. Millimeter-scale spatial variability in soil water sorptivity: Scale, surface elevation, and subcritical repellency effects. Soil Sci. Soc. Am. J. 68: 352-358.

Hangen, E., Gerke, H.H., Schaaf, W., and R.F. Hüttl. 2004. Flow path visualization in a lignitic mine soil using iodine-starch staining. Geoderma 120: 121-135.

Hangen, E., Gerke, H.H., Schaaf, W., and R.F. Hüttl. 2005. Assessment of preferential flow processes in a forest-reclaimed lignitic mine soil by multicell sampling of drainage water and three tracers. J. Hydrol. 303: 16-37.

Hartge, K.H. 1958. Die Wirkung des Kalkes auf die Strukturstabilität von Ackerböden. Dissertation. Department of Horticulture, Technical University of Hannover, Germany. *(in German)*

Hassanein, R., Lehmann, E., and P. Vontobel. 2005. Methods of scattering corrections for quantitative neutron radiography. Nuc. Instrum. Meth. Phys. Res. Sect. A 542: 353-360.

Hassanein, R., Meyer, H.O., Carminati, A., Estermann, M., Lehmann, E., and P. Vontobel. 2006a. Investigation of water imbibition in porous stone by thermal neutron radiography J. Phys. D: Appl. Phys. 39: 4284-4291.

Hassanein, R. 2006b. Correction methods for the quantitative evaluation of thermal neutron tomography. Ph.D. diss., Eidgenössische Technische Hochschule ETH Zürich, No. 16809, DOI: 10.3929/ethz-a-005273682.

Hastings, A., Byers, J.E., Crooks, J.A., Cuddington, K., Jones, C.G., Lambrinos, J.G., Talley, T.S., and W.G. Wilson. 2007. Ecosystem engineering in space and time. Ecol. Letters 10: 153–164.

Heil, J.W., Juo, A.S.R., and K.J. McInnes. 1997. Soil properties influencing surface sealing of some sandy soils in the Sahel. Soil Sci. 162: 459-469.

Hincapié, I., and P. Germann. 2009. Gravity-driven viscous flow in sand boxes assessed with neutron radiography. Vadose Zone J. 8: 891-901.

Holden, J., and K.F. Gell. 2009. Morphological characterization of solute flow in a brown earth grassland soil with cranefly larvae burrows (leatherjackets). Geoderma 152: 181-186.

Hüttl, R.F., and E. Weber. 2001. Forest ecosystem development in post mining landscapes: A case study of the Lusatian lignite district. Naturwissenschaften 88: 322-329.

Jarvis, N.J. 2007. A review of non-equilibrium water flow and solute transport in soil macropores: principles, controlling factors and consequences for water quality. Europ. J. Soil Sci. 58: 523-546.

Jasinska, E., Wetzel, H., Baumgartl, T., and R. Horn. 2006. Heterogeneity of physico-chemical properties in structured soils and its consequences. Pedosphere 16: 284-296.

Jégou, D., Cluzeau, D., Wolf, H.J., Gandon, Y., and P. Trehen. 1998. Assessment of the burrow system of Lumbricus terrestris, Aporrectodea giardi, and Aporrectodea caliginosa using X-ray computed tomography. Biol. Fertil. Soils 26: 116-121.

Jégou, D., Schrader, S., Diestel, H., and D. Cluzeau. 2001. Morphological, physical and biochemical characteristics of burrow walls formed by earthworms. Appl. Soil Ecol. 17: 165-174.

Jones, C.G., Lawton, J.H., and M. Shachak. 1994. Organisms as ecosystem engineers. Oikos 69: 373–386.

Jones, C.G., Lawton, J.H., and M. Shachak. 1997. Positive and negative effects of organisms as physical ecosystem engineers. Ecology 78: 1946–1957.

Kaestner, A., Hassanein, R., Vontobel, P., Lehmann, P., Schaap, J., Lehmann, E., and H. Flühler. 2007. Mapping the 3D water dynamics in heterogeneous sands using thermal neutrons. Chem. Eng. J. 130: 79-85.

Kaestner, A., Lehmann, E., and M. Stampanoni. 2008. Imaging and image processing in porous media research. Adv. Water Resour. 31: 1174-1187.

Kelln, C., Barbour, L., and C. Qualizza. 2007. Preferential flow in a reclamation cover: Hydrological and geochemical response. J. Geotech. Geoenviron. Eng. 133: 1277-1289.

Köhne, JM., Köhne, S., and J. Simunek. 2009. A review of model applications for structured soils: a) Water flow and tracer transport. J. Contam. Hydrol. 104: 4-35.

Koliji, A., Lehmann, P., Vulliet, L., Laloui, L., Carminati, A., Vontobel, P., and R. Hassanein. 2008. Assessment of structural evolution of aggregated soil using neutron tomography. Water Resour. Res. 44: W00C07.

Kramers, G., Richards, K.G., and N.M. Holden. 2009. Assessing the potential for the occurrence and character of preferential flow in three Irish grassland soils using image analysis. Geoderma 153: 362-371.

Langmaack, M., Schrader, S., and K. Helming. 2001. Effect of mesofaunal activity on the rehabilitation of sealed soil surfaces. Appl. Soil Ecol. 16: 121–130.

Lee, K.E., and R.C. Foster. 1991. Soil fauna and soil structure. Austral. J. Soil Sci. 29: 745-775.

Lee, S.S., Gantzer, C.J., Thompson, A.L., Anderson, S.H., and R.A. Ketcham. 2007. Using high-resolution computed tomography analysis to characterize soil-surface seals. Soil Sci. Soc. Am. J. 72: 1478-1485.

Lehmann, E.H., and P. Vontobel. 2000. Investigation of hydrogen distributions in various base materials by neutron radiography methods. Proceedings of the 15th World Conference on Non-Destructive Testing, Rome. p.1-12.

Lehmann, E.H., Vontobel, P., and N. Kardjilov. 2004a. Hydrogen distribution measurements by neutrons. Appl. Radiation Isotopes. 61: 503-509.

Lehmann, E.H., Vontobel, P., Frei, G., and C. Brönnimann. 2004b. Neutron imaging - Detector options and practical results. Nuc. Instrum. Meth. Phys. Res. Sect. A. 531: 228-237.

Lehmann, E.H., Vontobel, P., and G. Frei. 2005. Neutron imaging – Present status and options with TOF methods – TOF neutron imaging. J. Neutron Res. 13: 27-31.

Lehmann, P., Wyss, P., Flisch, A., Lehmann, E., Vontobel, P., Krafczyk, M., Kaestner, A., Beckmann, F., Gygi, A., and H. Flühler. 2006. Tomographical imaging and mathematical description of porous media used for the prediction of fluid distribution. Vadose Zone J. 5: 80-97.

Luo, L., Lin, H., and S. Li. 2010. Quantification of 3-D soil macropore networks in different soil types and land uses using computed tomography. J. Hydrol. 393: 53-64.

Malmström, M.E., Berglund, S., and J. Jarsjo. 2008. Combined effects of spatially variable flow and mineralogy on the attenuation of acid mine drainage in groundwater. Appl. Geochem. 23: 1419-1436.

Mannes, D., Niemz, P., and E. Lehmann. 2006. Study on the penetration behavior of water in corner joints by means of neutron radiography. Wood Res. 51: 1-14.

Maurer, T., and H.H. Gerke. 2011. Modelling aeolian sediment transport during initial soil development on an artificial catchment using WEPS and aerial images. Soil Tillage Res. 117: 148-162.

McFadden, L.D., McDonald, E.V., Wells, S.G., Anderson, J.Q., and S.L. Forman. 1998. The vesicular layer and carbonate collars of desert soils and pavements: formation, age and relation to climate change. Geomorphology 24: 101-145.

Menon, M., Robinson, B., Oswald, S.E., Kaestner, A., Abbaspour, K.C., Lehmann, E., and R. Schulin. 2007. Visualization of root growth in heterogeneously contaminated soil using neutron radiography. Eur. J. Soil Sci. 58: 802-810.

Miller, D.E., 1971. Formation of vesicular structure in soil. Soil Sci. Soc. Amer. Proc. 35: 635-637.

Mohamed, D., and R.A. Kohl. 1987. Infiltration response to kinetic energy. Trans. ASAE 30: 108-111.

Moradi, A.B., Conesa, H.M., Robinson, B., Lehmann, E., Kuehne, G., Kaestner, A., Oswald, S., and R. Schulin. 2009. Neutron radiography as a tool for revealing root development in soil: Capabilities and limitations. Plant Soil 318: 243-255.

Müller-Kroehling, S., Grünwald, M., and E. Scheuchl. 2000. Wiederfund von Cicindina arenaria viennensis (Schrank, 1781) in Bayern und

Umsiedlungsversuch aus dem bedrohten Lebensraum. Angewandte Carabidologie 2/3: 81-89. (in German)

Niessner, J., and R. Helmig. 2007. Multi-scale modeling of three-phase-three-component processes in heterogeneous porous media. Adv. Water Resour. 30: 2309-2325.

Nunan, N., Ritz, K., Rivers, M., Feeney, D.S. and I.M. Young. 2006. Investigating microbial micro-habitat structure using X-ray computed tomography. Geoderma 133: 398-407.

Otsu, N. 1979. A threshold selection method from grey-level histograms. IEEE Trans. Syst. Man. Cybern. 9: 62-66.

Peth, S., Horn, R., Beckmann, F., Donath, T., Fischer, J., and A.J.M. Smucker. 2008. Three-dimensional quantification of intra-aggregate pore-space features using synchrotron-radiation-based microtomography. Soil Sci. Soc. Am. J. 72: 897-907.

Pleinert, H., Sadouki, H., and F.H. Wittmann. 1998. Determination of moisture distributions in porous materials by neutron transmission analysis. Mater. Struct. 31: 218-223.

Prasse, R., and R. Bornkamm. 2000. Effect of microbiotic soil surface crusts on emergence of vascular plants. Plant Ecol. 150: 65-75.

Rasband, W.S. 1997-2009. ImageJ, U. S. National Institutes of Health, Bethesda, Maryland, USA, http://rsb.info.nih.gov/ij/.

Ribolzi, O., Patin, J., Bresson, L.M., Latachack, K.O., Mouche, E., Sengtaheuanghoung, O., Silvera, N., Thiebaux, J.P., and C. Valentin. 2011. Impact of slope gradient on soil surface features and infiltration on step slopes in northern Laos. Geomorphology 127: 53-63.

Romkens, M.J.M. 1979. Soil crusting – when crusts form and quantifying their effects. In Infiltration research planning workshop, Part I. State of the art reports. USDA-ARS.

Schaaf, W., Gast, M., Wilden, R., Scherzer, J., Blechschmidt, R., and R.F. Hüttl. 1999. Temporal and spatial development of soil solution chemistry and element budgets in different mine soils of the Lusatian lignite mining area. Plant Soil 213: 169-178.

Schaaf, W., and R.F. Hüttl. 2006. Direct and indirect effects of soil pollution by lignite mining. Water, Air and Soil Pollut.-Focus 6: 353-364.

Schaaf, W., Biemelt, D., and R.F. Hüttl (Eds.). 2010): Initial development of the artificial catchment "Chicken Creek" - monitoring program and survey 2005-2008. URN: urn:nbn:de:kobv:co1-opus-20732.

Schaaf, W., Bens, O., Fischer, A., Gerke, H.H., Gerwin, W., Grünewald, H., Holländer, H.M., Kögel-Knabner, I., Mutz, M., Schloter, M., Schulin, R., Veste, M., Winter, S., and R.F. Hüttl. 2011. Patterns and processes of initial terrestrial-ecosystem development. J. Plant Nutrition Soil Sci. 174 (2): 229-239.

Schaap, J.D., Lehmann, P. , Kaestner, A., Vontobel, P., Hassanein, R., Frei, G., de Rooij, G.H., Lehmann, E., and H. Flühler. 2008. Measuring the effect of structural connectivity on the water dynamics in heterogeneous porous media using speedy neutron tomography. Adv. Water Resour. 31: 1233-1241.

Schrader, S., Rogasik, H., Onasch, I., and D. Jégou. 2007. Assessment of soil structural differentiation around earthworm burrows by means of X-ray computed tomography and scanning electron microscopy. Geoderma 137: 378-387.

Schulin, R., Wierenga, P.J., Flühler, H., and J. Leuenberger. 1987. Solute transport through a stony soil. Soil Sci. Soc. Am. J. 51: 36-42.

Six, J., Bossuyt, H., Degryze, S., and K. Denef. 2004. A history of research on the link between (micro)aggregates, soil biota, and soil organic matter dynamics. Soil Tillage Res. 79: 7-31.

Smucker, A.J.M., Park, E.J., Dorner, J., and R. Horn. 2007. Soil micropore development and contributions to soluble carbon transport within macroaggregates. Vadose Zone J. 6: 282-290.

Springer, M.E. 1958. Desert pavement and vesicular layer of some soils of the desert of the Lahontan Basin, Nevada. Soil Sci. Soc. Am. Proc. 22: 63-66.

Tschapek, M., Scoppa C.O., and C. Wasowski. 1978. The surface tension of soil water. J. Soil Science 29: 17-21.

Tschumperlé, D., and R. Deriche. 2003. Vector-Valued Image Regularization with PDE's: A Common Framework for Different Applications. CVPR2003 - IEEE Conference on Computer Vision and Pattern Recognition , Madison/USA.

Tumlinson, L.G., Liu, H.Y., Silk, W.K., and J.W. Hopmans. 2008. Thermal neutron computed tomography of soil water and plant roots. Soil Sci. Soc. Am. J. 72: 1234-1242.

Turk, J.K., and R.C. Graham. 2011. Distribution and properties of vesicular horizons in the western united states. Soil Sci. Soc. Amer. J. 75: 1449-1461.

Valentin, C. 1991. Surface crusting in two alluvial soils of northen Niger. Geoderma 48: 201-222.

Valentin, C., and L.-M. Bresson. 1992. Morphology, genesis and classification of surface crusts in loamy and sandy soils. Geoderma 55: 225-245.

Vasin, M., Lehmann, P., Kaestner, A., Hassanein, R., Nowak, W., Helmig, R., and I. Neuweiler. 2008. Drainage in heterogeneous sand columns with different geometric structures. Adv. Water Resour. 31: 1205-1220.

Vereecken, H., Kasteel, R., Vanderborght, J., and T. Harter. 2007. Upscaling hydraulic properties and soil water flow processes in heterogeneous soils: A review. Vadose Zone J. 6: 1-28.

Vinegar, H.J., and S.L. Wellington. 1987. Tomographic imaging of three-phase flow experiments. Rev. Sci. Instrum. 58: 96-107.

Vogel, H.J., and K. Roth. 2003. Moving through scales of flow and transport in soil. J. Hydrol. 233: 95-106.

Vontobel, P., Lehmann, E.H., Hassanein, R., and G. Frei. 2006. Neutron tomography: Method and applications. Physica B 385: 475-480.

Vontobel, P., Hassanein, R., Carminati, A., Kaestner, A., Lehmann, P., and A. Koliji. 2008. Neutron imaging for soil physics and geology. Neutron Radiography p.369-373.

Yonovitz, M., and P.J. Drohan. 2009. Pore morphology characteristics of vesicular horizons in undisturbed and disturbed arid soils; implications for arid land management. Soil Use and Management 25: 293-302.

Young, M.H., McDonald, E.V., Caldwell, T.G., Benner, S.G., and D.G. Meadows. 2004. Hydraulic properties of a desert soil chronosequence in the Mojave Desert, USA. Vadose Zone J. 3: 956-963.

Weiler, M., and F. Naef. 2003. An experimental tracer study of the role of macropores in infiltration in grassland soils. Hydrol. Process. 17: 477-493.

Werth, C.J., Zhang, C.Y., Brusseau, M.L., Oostrom, M., and T. Baumann. 2010. A review of non-invasive imaging methods and applications in contaminant hydrogeology research. J. Contam. Hydrol. 113: 1-24.

WRB. 2006. World reference base for soil resources. 2nd edition. World Soil Resour. Rep. 103. FAO, Rome.

Wright, J.P., and C.G. Jones. 2006. The concept of organisms as ecosystem engineers. Ten years on: progress, limitations and challenges. Bioscience 56: 203–209.

7. Summary

The term ‘preferential’ or ‘non-equilibrium flow’ in soils describes the complex hydrological process of water transport in porous media showing a high local variability. The occurrence of preferential flow is rather the rule than the exception particularly in heterogeneous structured soils. The quantitative prediction is difficult because of the spatial as well as temporal variability. Furthermore, measurements are experimentally demanding because of the variable scale of these flow domains, particularly the small spatial extent of highly conductive pore systems.

One aim of the dissertation was to visualize the soil structure and flow patterns in mine soils with differently formed pore networks using a combination of neutron radiography, neutron tomography and x-ray computed tomography experiments. Both radiation techniques were used to describe preferential pathways as a soil structure with CT and the process of preferential flow of water with NT. For the first time neutron radiation was applied on undisturbed soil cores to visualize water distributions in natural soils on three examples for heterogeneities of different origin.

I. In a first investigation we used neutron radiography to analyze the moisture distribution in undisturbed slab-type and cylindrical samples of mine soils containing lignitic fragments and inclined layers. Two-dimensional (2D) radiographs of steady-state infiltration experiments in unsaturated (i.e., -5 hPa) soil slabs were used to study the dynamics of 2D moisture patterns. With another experimental setup, attempts were carried out utilizing neutron tomography to determine three-dimensional (3D) water content distributions for stationary phases of one-step in- and outflow experiments under near-saturated (i.e., -3 to -30 hPa) conditions on undisturbed soil cores. Inside the soil cores, miniature tensiometers were installed to monitor the pressure head dynamics in contrasting pore regions (i.e., fragments and sandy matrix). In the 2D slab-type samples, even relatively narrow (mm-scale) flow paths could be distinguished and visualized. The 2D radiography sequences indicated that flow pathways are highly dependent on the shape, distribution, and internal structure of the lignitic fragments. For the 3D experiments, the quantitative analysis of water contents failed due to a

pronounced beam hardening effect. The tensiometer data indicated the existence of local non-equilibrium in pressure heads between fragments and matric pore regions. Nevertheless, the 3D information could qualitatively be compared with those of the 2D results. The results from both methods analogously suggest that under near-saturated conditions, water flow takes places around the lignitic fragments and within a second continuous pore network within the lignitic dust containing sandy matrix.

II. The objective of the second study was to analyze and visualize the effects of initial soil structure formation at the surface of bare soils in an artificial hydrological catchment that has been left to undirected ecological succession for three years. The three-dimensional (3D) micro-morphology was described using the X-ray computed tomography (CT); two-dimensional (2D) infiltration patterns were obtained from drip infiltration experiments using time-resolved neutron radiography (NT). The soil samples were taken from three locations representing the main sediment types of the heterogeneous sediments of the catchment. The analyses of CT data indicate the existence of (i) structural crusts on soil consisting of sandy to loamy sediments and (ii) depositional crusts on sandy sediments. In locations dominated by silty to fine-sand sediments soil, a combination of these two types developed, probably as a result of aeolian deposition on a structural crust. Moreover, isolated vesicle-shaped pores were observed in most samples. The 2D infiltration patterns reflected the structural alteration by crusts only in the samples that contained the silty soil: Infiltrating water tended to pond within the aeolian fine sand deposits above the underlying structural crust. For all other samples, relatively uniform 2D infiltration patterns and little effect of the crusts or the vesicular pores on infiltration and redistribution could be observed. The results of combined observations using CT and NT suggest that the initial soil surface structure alterations of young sandy sediment modify moisture patterns of infiltrating water only slightly.

III. The aim of the 3rd experiment was to study effect of two ‘ecological engineers’, moss vegetation and beetle larvae on pore structure and infiltration. The soil pore structure was characterized by micro-computed tomography analyses of bare soil, sparse and dense moss-vegetated samples containing a single burrow. Flow patterns of infiltration experiments were visualized using the neutron radiography

technique. The micro-CT scans revealed differences in soil structure ranging from an extended unstable pore system in the bare soil to a locally compacted soil surface in the moss-covered sample. Moreover, many isolated vesicular pores were observed in the vegetated samples, what had been reported for desert soils before. The neutron radiograph series showed a flow around the cylindrical burrow under initially moist, and pronounced preferential flow within the burrow under initially dry soil conditions. The bottom part of the dry radiography sample revealed water repellent regions which probably acted as a barrier for capillary flow and explained a water pressure build-up in the upper soil regions near the surface; pressure was eventually released when water could laterally entered the biopore and gravity-driven flow in the burrow started. Another effect of the moss cover could be the inhibition of soil erosion due to the stabilization of the soil surface by their roots, visible in the absence of a depositional sediment layer on top of the samples. The results of this study suggest that moss vegetation and burrowing activity of ground beetles strongly control the initial soil development by modification of pore structure and surface water infiltration.

The presented experiments on flow patterns in differently structured mine soils reflect the inherent heterogeneity of the investigated soils. The combination of visualization techniques quantifying the structure and the flow patterns played here the key role for understanding the observed flow processes. Here, neutron radiography firstly proved as a suitable method also for undisturbed natural soil samples for the first time.

8. Acknowledgements

I would like to thank Professor Reinhard F. Hüttl for the continuous support of my Ph.D study and related research. I highly appreciate the access to the state-of-the-art laboratory and research facilities of the Chair of Soil Protection and Recultivation.

I would like to express my special appreciation and thanks to my supervisor Dr. Horst Gerke for his patience, encouraging my research and for allowing me to grow as a research scientist. Without his precious support it would not be possible to conduct this research.

My sincere thanks also go to my colleges and technicians in the different research projects for the stimulating discussions and insightful comments, and for all the fun we have had in the last years.

This study was part of the Transregional Collaborative Research Center 38 (SFB/TRR 38, ‘‘Structures and processes of the initial ecosystem development phase in an artificial water catchment’’, subproject A4) which was financially supported by the Deutsche Forschungsgemeinschaft (DFG, Bonn) and the Brandenburg Ministry of Science, Research and Culture (MWFK, Potsdam).

For the non-scientific side of my thesis, I particularly want to thank my parents and my brother for supporting me spiritually throughout writing this thesis and my life in general.